

77P

NASA CR 174819

(NASA-CR-174819) EFFECT OF ANGULAR INFLOW
ON THE VIBRATORY RESPONSE OF A
COUNTER-ROTATING PROPELLER (Hamilton
Standard, Windsor Locks, Conn.) 75 p

N87-10840

CSCCL 01A G3/02

Unclas
43847



**EFFECT OF ANGULAR INFLOW ON THE VIBRATORY RESPONSE
OF A COUNTER-ROTATING PROPELLER**

by

J.E. Turnberg

P.C. Brown

**HAMILTON STANDARD DIVISION
UNITED TECHNOLOGIES CORPORATION**

Prepared For

NATIONAL AERONAUTICS AND SPACE ADMINISTRATION

**Lewis Research Center
Cleveland, Ohio 44135**

Contract NAS3-24222



**EFFECT OF ANGULAR INFLOW ON THE VIBRATORY RESPONSE
OF A COUNTER-ROTATING PROPELLER**

by

J.E. Turnberg

P.C. Brown

**HAMILTON STANDARD DIVISION
UNITED TECHNOLOGIES CORPORATION**

Prepared For

NATIONAL AERONAUTICS AND SPACE ADMINISTRATION

**Lewis Research Center
Cleveland, Ohio 44135**

Contract NAS3-24222

FOREWORD

The experimental and analytical effort described in this report was conducted by the Hamilton Standard Division of the United Technologies Corporation under NASA contract NAS3-24222. Mr. Irving E. Sumner of the NASA Lewis Research Center was the Technical Monitor for the contract.

This report was prepared by Mr. Jay E. Turnberg and Mr. Paul C. Brown under the direction of Mr. David E. Sladewski, Hamilton Standard Project Manager.

TABLE OF CONTENTS

Section		Page
1.0	SUMMARY	1
2.0	INTRODUCTION	3
3.0	DISCUSSION	5
	3.1 Test Bed Aircraft	5
	3.2 Blade Description and Instrumentation	6
	3.2.1 Blade Measurements	6
	3.2.2 Strain Gage Locations	8
	3.2.3 Instrumentation	8
	3.3 Test Conditions	10
	3.4 Experimental Results	11
	3.4.1 Stabilized Flight	11
	3.4.1.1 Counter-Rotation vs Single-Rotation	11
	3.4.1.2 Blade Stress Distribution	12
	3.4.1.3 Torsional Response	13
	3.4.2 Yaw Maneuvers	13
	3.4.3 Pitch Maneuvers	15
	3.4.4 Campbell Plots	16
	3.5 Analytical Predictions	17
	3.5.1 Conditions Examined	17
	3.5.2 Counter-Rotation Analysis	18
	3.5.3 Counter-Rotation vs Single-Rotation	18
	3.5.4 Single-Rotation Analysis	19
4.0	CONCLUSIONS	21
5.0	RECOMMENDATIONS	23
6.0	REFERENCES	23

1.0 SUMMARY

The emergence of the Prop-Fan as a fuel conservative competitor to the high by-pass ratio turbofan has created new interest in propeller technology development. Both analytical studies and wind tunnel tests have shown that efficiencies of about 80 percent are achievable at flight Mach numbers of 0.7 to 0.8 for single-rotation Prop-Fans. In achieving these high efficiencies the single-rotation Prop-Fan imparts a high velocity swirl to the flow that represents an energy loss. The energy in the swirl can be recovered by a counter-rotating Prop-Fan for which efficiencies on the order of 90 percent can be achieved. The intent of this program is to provide a preliminary assessment of the effect of counter-rotation on the structural response of a propeller to angular inflow. To assess the effects of counter-rotation, Hamilton Standard purchased and flight tested a Fairey Gannet aircraft which is powered by a counter-rotating propeller and has the unique capability of operating each propeller blade row independently.

The results of the structural tests showed that counter-rotating operation of the propeller has the effect of increasing the 1P (once per revolution) response of the rear propeller by approximately 25 percent while having essentially no influence on the 1P response of the front propeller. For the Gannet installation the higher order response was not significant, but in general the effect of counter-rotation was to increase the response of both blades. Analytical predictions of the propeller response show varying degrees of correlation with test data. The variation in the predicted results is attributed to deficiencies in the theoretical approach, inaccuracies in defining the modeled operating conditions, and inaccuracies in the experimental process. The definition of the operating condition becomes increasingly important as flight speed increases because the response is more sensitive to variations in pitch and yaw angles at high speed, and for this installation the magnitude of the response decreases with increased flight speed and experimental accuracy decreases. Further work should be performed to refine the analytical methodology using the Fairey Gannet low speed response data for guidance.

2.0 INTRODUCTION

The emergence of the Prop-Fan as a fuel conservative competitor to the high by-pass ratio turbofan has created new interest in propeller technology development. Both the analytical studies and wind tunnel tests have shown that efficiencies of about 80 percent are achievable at flight Mach numbers of 0.7 to 0.8 where single-rotation Prop-Fans (SRP) are intended for operation. Although the Prop-Fan is lightly loaded in relation to a high by-pass ratio turbofan, it is highly loaded in relation to today's three and four bladed propellers which are designed for lower flight speeds. Loadings expressed as shaft power divided by the square of the rotor diameter at the cruise design point are about 2410 Kw/m² (300 hp/ft²) for a 1.60 pressure ratio turbofan, 240 Kw/m² (30 hp/ft²) to 320 Kw/m² (40 hp/ft²) for Prop-Fans and 80 Kw/m² (10 hp/ft²) to 120 Kw/m² (15 hp/ft²) for low speed application three and four bladed propellers. The turbofan has the smallest diameter and imparts the highest swirl velocity to the airstream. The swirl from the turbofan rotor is turned to the axial direction by a downstream row of stator blades. These stators convert swirl to a static pressure rise which appears as an increase in propulsive thrust and yields a cruise efficiency of about 65 percent. The lightly loaded three and four bladed propellers used in low-speed aircraft do not impart high swirl velocities and, as a result, do not have a significant amount of swirl-energy in the slipstream. Swirl velocities for the Prop-Fans are considerably higher than conventional propellers. Even with swirl losses, Prop-Fan cruise efficiencies of about 80% can be achieved, thus, yielding significant fuel use advantage over the turbofan.

Full recovery of the swirl energy by employing counter-rotation can improve the design point cruise efficiency over SRP by approximately 8 efficiency points yielding about 88% efficiency at cruise conditions. This efficiency improvement with counter-rotation Prop-Fans (CRP) has substantial potential for increased fuel savings and reduced DOC for aircraft. Results of a 1982 NASA study on CRP (Reference 1) showed that for a 120 passenger commercial aircraft operating at 0.8 Mach number, a 9% fuel savings and 3% reduction in DOC was realized over the identical optimal SRP powered aircraft.

The objective of this program was to provide an early assessment of counter-rotating propeller vibratory response by using Hamilton Standard's Fairey Gannet aircraft as a test bed for collecting counter and single-rotation propeller vibratory response data. Because of the aircraft's capability to operate each propeller independently the aircraft offers a direct comparison between counter and single-rotation operation. The resulting test data also serves to provide a data base for the refinement of analytical methodology and to provide guidance for future counter-rotating propeller research.

3.0 DISCUSSION

3.1 Test Bed Aircraft

Hamilton Standard purchased a Fairey Gannet A.E.W.3 counter-rotating propeller aircraft in April, 1983. This carrier based aircraft (Figure 1) was built by Fairey Aviation in the late 1950's and was on active duty until 1979. In 1982 the aircraft was completely refurbished according to the Royal Navy's military standards and flown to the United States. It is one of only a few known flyable Gannet aircraft in the world today and the only known available Gannet in the United States. This aircraft was of particular interest to Hamilton Standard not only for its counter-rotating propellers but also for the unique capability of the aircraft to operate each propeller row independently. The aircraft is powered by the Bristol Siddley Double Mamba power plant consisting of two gas turbines placed side by side each driving one of two coaxial counter-rotating propellers. The engines are entirely independent, each having its own fuel, lubrication and control system. The starboard engine drives the front propeller. The port engine drives the rear propeller. A common auxiliary gearbox is driven by either engine or both which enables the pilot to stop one of the engines and feather its propeller in flight. This was originally designed into the aircraft to reduce fuel consumption and increase surveillance flight time. This capability was to be utilized to its fullest advantage in the structural test program.

Hamilton Standard's Gannet was modified in June 1983 at the United Technologies Corporation's experimental hanger in preparation for an in-house funded acoustic test program. A 5.18 meter (17 ft) boom was attached to the port wing jacking points (Figure 2). The boom cantilevers forward to the propeller plane of rotation where yaw and pitch instrumentation was attached to measure angular inflow into the propellers for this flight test program. Signal conditioning and recording equipment was secured in the aft section of the aircraft where shock mounted shelves previously secured the Gannet's Airborne Early Warning Radar. The electrical supply for the instrumentation was available in a variety of locations because of its original radar capability.

A brief description of the Fairey Gannet aircraft characteristics includes the following:

Engine Characteristics

Siddley Double Mamba 2759 KW (3700 SHP), MAX. RPM = 15,000, 0.0874:1 gear ratio, 11 stage axial compressor @ 5.75:1 compression ratio, 19.05 Kg/sec (42 lb/sec) inlet airflow, annular combustion chambers, 3 stage axial turbine 1397 Kg (3080 lb) engine weight, dry.

Aircraft Dimensions

Height to top of fin	5.11M (16.8 ft)
Height required for folding wings	5.41M (17.8 ft)
Height to top of folded wings	5.08M (16.7 ft)
Length overall (including hook)	13.39M (43.9 ft)
Span	16.64M (54.6 ft)
Maximum width, wings folded	6.10M (20.0 ft)
Span of tailplane	5.94M (19.5 ft)

PerformanceMaximum Speeds

Diving (clean)	519 Km/hr (280 knts)
Flaps down	250 Km/hr (135 knts)
Raising and lowering landing gear	278 Km/hr (150 knts)
Flight with landing gear down	296 Km/hr (160 knts)
With drop tanks or starter pod	444 Km/hr (240 knts)
Radome and radar antenna removed	370 Km/hr (200 knts)

Weights

Normal maximum take-off weight	10544 Kg (23,245 lbs)
Maximum permissible takeoff weight	11794 Kg (26,000 lbs)
Maximum permissible landing weight	11703 Kg (25,800 lbs)

3.2 Blade Description and Instrumentation3.2.1 Blade Measurements

To investigate the vibratory response of the Fairey Gannet 4 x 4 counter-rotating propellers, a detailed description of the front and rear

blades was required. This was accomplished by using a spare set of Gannet propeller blades. The front and rear blades were disassembled from the barrels which enabled blade measurements and frequency tests to be performed.

The blade removal process proved to be complex since the blades were threaded into the barrel with 10,645 N-M (7850 ft-lbs) of torque. Special tooling had to be designed and fabricated in order to safely unscrew the blades. Upon removal of the blades, measurements were made of the blade section profiles so that appropriate section properties could be developed.

The measurements were obtained at 25.4 CM (10 in.) increments from the blade tip except in the regions near the blade shank and tip where large transitions in geometry occurred over small radial increments. Additional measurements were taken in these transition regions.

Visual inspection of the front and rear blades had initially indicated that they were very close to each other in geometry. This cursory evaluation did not hold up upon detailed evaluation. Figure 3 shows the geometric differences between the two types of blades. The front blade was 3.81 CM (1.5 in.) longer than the rear blade because the front barrel was smaller in diameter. This allows the front and rear propellers to have the same overall diameter of 3.76M (148 in.). The front blade was generally wider and thicker. These differences were greatest over the inboard half of the blades. Figure 3 also shows a curve representing equivalent 16 series airfoil camber represented as design lift coefficient, C_{ld} . Equivalent camber is shown because these airfoils were not 16 series airfoils. The true configuration was not determined because a 16 series airfoil with the proper camber provided a good representation of the measured airfoil shape. Figure 4 shows a comparison between a measured Gannet propeller blade cross-section and a 16 series airfoil with an equivalent amount of camber. The equivalent 16 series representation was generally good. Important structural features that were maintained with the representation were overall mid-chord thickness and chord length. Measurements of mid-chord thickness and chord length from the flight tested blades were compared to the spare blade measurements to confirm similarity between the spare blades and flight tested blades.

From the blade section descriptions, two analytical beam models were generated for the purpose of calculating the modal and response data required for the selection of strain gage locations and comparison to test results. Tables I and II give the beam section property data developed for the front and rear blades. To verify the representation of the blades, static modal frequencies were calculated using the analytical models, and a comparison was made with the measured frequencies. Table III shows a comparison between the measured and calculated frequencies. The comparison is generally good verifying that the blade modeling procedure was satisfactory.

The static modal frequency measurements noted in Table III were obtained by clamping each blade in a test fixture, Figure 5, and shaking the blades over a frequency range to determine their natural frequencies. The test set-up is shown by the installation photograph, Figure 6. To provide a solid foundation to clamp each blade, the entire retention area, at the blade root, was potted in lead and clamped in the test shake fixture. This method of clamping circumvented the need for special fixtures and tools to remove the pitch bearing and clamp the blade in the test fixture.

3.2.2 Strain Gage Locations

In addition to calculating the modal frequencies for the front and rear blades, stress mode shapes and preliminary vibratory response stresses were determined in order to locate the strain gages. Figures 7 and 8 show normalized stress distributions for each blade, front and rear. The purpose of selecting the strain gage locations for these blades was to give informative data concerning the vibratory response of the counter-rotating propeller. Examination of Figures 7 and 8 shows that a bending gage at the 50.8 CM (20 in.) station would respond well to 1P loads, the first bending mode (1F, first flatwise mode), and possibly 8P loads. A bending gage at the 129.5 CM (51 in.) would respond to the second bending mode (2F, second flatwise mode), and a bending gage at the 160 CM (63 in.) station would respond to the third bending mode (1E, first edgewise mode) and possibly 8P loads. The vee gage located at the 129.5 CM (51 in.) station was placed to respond to the first torsion mode. Four gages were also installed on the blade shanks in push-pull pairs for the purpose of obtaining 1P, 1F, and 1E shank bending moment response. Shank gages were applied to the blade adjacent to the fully gaged blade in both the front and rear blade rows for the purpose of obtaining response phase relationships. The calculated direction of the 1P shank bending moment was used to orient the shank gages so that the flatwise shank gages would respond predominantly to 1P loads. Figures 9 and 10 show the gage installations for the instrumented front and rear row blades and Table IV lists gage designations and installation instructions.

3.2.3 Instrumentation

The data acquisition system for the Fairey Gannet aircraft was designed to record all required data and to integrate with the existing aircraft hardware and electronics. The following measurements, sensors, and ranges were employed:

<u>Measurement</u>	<u>No.</u>	<u>Sensor</u>	<u>Range</u>
Blade Strain	(16)	Strain gage	$\pm 2000 \mu \epsilon$
Once/Rev.	(2)	Magnetic pickup	-
Aircraft C.G.	(1)	Accelerometer	$\pm 2g$
Aircraft Pitch	(1)	Boom mounted pot	$\pm 180^\circ$
Aircraft Yaw	(1)	Boom mounted pot	$\pm 180^\circ$

The transmission of data from the rotating to nonrotating reference frame was accomplished using the existing propeller de-icing slip rings modified for data transmission and rotating electronics. The front propeller has three slip rings and the rear propeller has five slip rings. These slip rings were utilized as follows:

<u>Front Slip Ring</u>	<u>Utilization</u>
1	Power Front Propeller
2	Front 1P Intra-Propeller Signal
3	Front Strain Gage Signals
<u>Rear Slip Ring</u>	<u>Utilization</u>
1	Power Front Propeller
2	Power Rear Propeller
3	Front 1P Intra-Propeller Signal
4	Rear 1P Signal
5	Front & Rear Strain Gage Signals

Two propeller mounted FM (frequency modulated) data acquisition systems as shown in Figures 11 and 12 were used to obtain strain gage data from the front and rear propellers. The use of an FM system allowed all 16 strain gage signals to be transmitted over one slip ring. The front propeller's rotating amplifiers and voltage controlled oscillators (VCO) convert the 8 front propeller strain gage signals into a frequency spectrum of 8 constant bandwidth channels from 14K Hz to 74K Hz which was transmitted across the slip ring to the rear propeller where the front blade signal was combined with the rear blade strain gage signal. The rear blade strain gage signals were similarly converted to an FM signal in the 78K Hz to 138K Hz range.

In the non-rotating reference frame the FM signal containing all 16 strain gage channels was translated into four groups of four strain gage channels for recording. These groups contain the same frequency structure. In addition to the four groups of strain gage records the following additional information was recorded:

Front propeller 1P intra-propeller-speed-phase-pip

Rear propeller 1P speed-phase-pip

Pitch angle of the aircraft

Yaw angle of the aircraft

Vertical acceleration of the aircraft C.G. (Nz)

Observer's voice

IRIG B Time Code

The following information was noted in a log for steady-state conditions and at key points during transient conditions.

Run number	Rear propeller power
Front propeller speed	Indicated airspeed
Rear propeller speed	Altitude
Front propeller power	

3.3 Test Conditions

A series of test conditions were established for the Gannet installation to assess the effect of angular inflow on the response of a counter-rotating propeller. The test conditions included ground operation, stabilized flight, and mild maneuvers over a range of power, airspeed, and propeller speed. The ground operation conditions were specified in the test plan for the purpose of refining the structural model. Random aerodynamic turbulence on the ground tends to excite natural blade modes that can then be identified and compared with analytical blade predictions.

The stabilized flight conditions which comprised the majority of the test provided the primary data used to assess the difference between counter and single-rotation operation. Single-rotation operation of either front or rear propeller involved shutting down operation of the other propeller and feathering it. Counter-rotation operation of both propellers involved the use of both propellers at the same speed and with either the same or varying amounts of power applied to each. Table V contains the log of the stabilized flight conditions. At each stabilized flight airspeed the aircraft was either in a dive, climb, or level flight condition to achieve the required airspeed. Also, each airspeed was associated with a specific pitch of the aircraft because the aircraft gross weight was not changed during the test.

To change the aircraft pitch at a particular airspeed, the gross weight must be changed. A gross weight change was simulated with roller coaster maneuvers where the relative g-level was changed during pullout and pushover maneuvers. Table VI shows a summary of the roller coaster maneuvers. The

inflow to the propellers was also altered by side-slip maneuvers in which the yaw of the aircraft with respect to the flight direction was varied. Table VII shows a summary of the side-slip maneuvers performed. The test results from the flight test will be discussed in the next section.

3.4 Experimental Results

3.4.1 Stabilized Flight

3.4.1.1 Counter-Rotation vs Single-Rotation - Stabilized flight data for the Gannet counter-rotating propeller installation showed that counter-rotation adversely affected the response of the rear blade due to angular inflow. Figures 13 and 14 show a comparison of total flatwise blade shank moments between counter-rotation and single-rotation propeller operation. Figure 13 shows that differences between counter and single-rotation response of the front blade was within the scatter of the test data whereas Figure 14 shows that the flatwise moment of the rear blade was significantly raised by counter-rotation operation. This front and rear blade response trend was also exhibited by blade 2 of the propellers further supporting the results from the blade 1 data. The blade 2 results are shown by Figures 15 and 16.

Spectral analysis of the signals for the low speed 222 Km/hr (120 knts) and high speed 370 Km/hr (200 knts) single and counter-rotating data uncovered the following trends in the response. On the front blade counter-rotation did not raise the 1P shank moment but significantly raised the 2P shank moment response as shown by Figures 17 and 18. This trend indicates that the rear propeller has little effect on modifying the angular inflow to the front propeller causing 1P response. However, the rear propeller does produce a 2P disturbance in the flow field that increases the front blade 2P response.

The effect of counter-rotation on the rear blade was different than on the front blade. Counter-rotation increased the 1P response of the rear blade while it did not change the 2P blade response as shown in Figures 17 and 18. The higher 1P of the rear blade during counter-rotating operation indicated that the front propeller significantly disturbs the angular inflow into the rear propeller such that the 1P aerodynamic loads increase. The lack of change of rear blade 2P response implies that the influence of aircraft asymmetry was the factor in determining the 2P response, not the influence of the front propeller. The only significant flatwise blade shank moment existing at a frequency greater than 2P occurred on the rear blade in high speed flight when the front blade was feathered and not rotating. When the front blade was stopped it became a stator and caused a 4P excitation on the rear propeller. This effect is displayed in Figure 18.

The front blade stator effect put a bias in the total vibratory moment for the rear blade as results shown in Figures 14 and 16. Therefore, the test data was band-pass filtered at 1P so that the effect of counter-rotation on 1P response could be assessed on an equivalent single and counter-rotation

basis. It should also be noted that some persistent lower frequency noise, below 1P, was evident in all the data. The exact nature of the noise is not known but it was assumed to be due to the onboard aircraft electronics. The 1P moment data for the front and rear blade is shown in Figures 19 and 20. Band pass filtering the data at 1P had the effect of lowering the single-rotation response of the rear blade at high speeds which resulted in a larger separation between the counter and single-rotation data.

In addition to the blade on/off operation in stabilized flight, the power was changed in each blade row so that the effect of mis-matched power could be assessed. The mis-matched power results are shown in Figures 21 and 22 for the cases where the front blade power was held constant while the rear blade power was varied and where the rear blade power was held constant while the front blade power was varied. The results show that the rear blade shank moment was affected by changes in front blade power more than the front blade was affected by the rear blade power. This result supports the earlier observation that the rear blade was more affected by counter-rotation operation than the front blade.

Blade edgewise response was also recorded during testing with the shank edgewise bending gages on the front and rear propellers. The edgewise response was significantly lower than the blade flatwise response as shown in Figures 23 and 24. In all cases, except for single-rotation operation on the front propeller, the 2P edgewise response was the largest component of the total edgewise vibratory response. Since the edgewise response was low no further discussion will be made concerning the details of the edgewise response.

3.4.1.2 Blade Stress Distribution - The Gannet blade bending stresses were recorded by the three bending gages at the 50.8CM (20 in.), 129.5CM (50 in.) and 160CM (63 in.) stations (inboard, mid-blade, and tip bending gages). For the high and low speed conditions the recorded data was spectral analyzed to assess the frequency content of the stresses in counter and single-rotation configurations. Figures 25 thru 30 show the bending stress spectral plots for the cases;

<u>Low Speed 222 Km/hr (120 Knts)</u>	<u>High Speed 370 Km/hr (200 Knts)</u>
CRP Front Run 1	CRP Front Run 8
SRP Front Run 13	SRP Front Run 17
CRP Rear Run 9	CRP Rear Run 8
SRP Rear Run 1	SRP Rear Run 8

Briefly, the inboard bending gages show results that are similar to the blade shank gages. The response was dominated by the 1P harmonic, and the rear blade 1P response was adversely affected by counter-rotation whereas the front blade 1P response was relatively unaffected by counter-rotation. Also, throughout the single-rotation data the 4P was biased by the effect of the front or rear non-rotating blade acting as a stator and increasing the 4P blade excitation. The blade response at the mid-blade gage and tip gage showed increasingly higher P order response relative to the 1P. This increase in higher order response towards the blade tip is normal for propeller response. The amplitude of the 1P, 2P, and 8P response has been plotted as a function of airspeed in Figures 31 thru 33 so that trends with airspeed, radial location and single vs counter-rotation can be assessed. Figure 31 shows that 1P decreased with airspeed for all gages and modes of operation. Also the 1P stress decreased radially towards the blade tip. The figure also illustrates the effect that counter-rotation has on the rear blade and the lack of effect on the front blade.

For this installation the 2P response generally increases with airspeed. In most cases the 2P response was higher for the counter-rotating configuration on both front and rear blades as shown in Figure 32.

Figure 33 shows the 8P response which was higher for all counter-rotating cases examined on both front and rear blades. Also, the 8P response tends to increase toward the blade tip. The high frequency modes of the blade were excited by 8P and showed more response at the blade tip. Whereas the low frequency modes were excited by 1P showed more response at the blade root.

3.4.1.3 Torsional Response - The highest response to the 8P blade passage frequency was exhibited by the torsion modes of the blade. The rear blade had a torsional natural frequency of 160 Hz and the front blade had a torsional natural frequency of 182 Hz where the 8P excitation frequency was in-between at 175 Hz. Figures 34 and 35 show the comparison between 8P for the counter and single-rotation configurations. For the counter-rotating configuration the 8P response in torsion was the largest component comprising the torsional response. The one peculiar aspect of data was the appearance of an 8P excitation in the rear blade of the single-rotation installation. The 8P response may have been a harmonic of the 4P impulsive wake loading due to the non-rotating front blade acting like an upstream stator.

3.4.2 Yaw Maneuvers

Two yaw maneuvers were performed during flight testing, the first a low speed 259 Km/hr (140 knt) and the second a high speed 333 Km/hr (180 knt) run. Each yaw maneuver had two events, a yaw left and a yaw right where each turn was varied from 0 to 10 degrees. Both low speed and high speed maneuvers were performed with Gannet propellers counter-rotating with both front and rear propellers operating at 1300 RPM.

Figure 36 is a plot of total vibratory flatwise shank moment versus yaw angle for the low speed case, Figure 37 is the same plot for the high speed case. Both figures show that vibratory shank moment was a hyperbolic function of yaw angle.

Two points about the relationship between the front and rear vibratory shank moments can be made after studying these yaw maneuver plots. One, the rear blade experiences higher moments over the range of yaw angles tested (omitting the effect of horizontal offset). Two, the horizontal offset or skewing of the rear blade curve represented some unexplained flow disturbance, experienced by the rear blade row.

There were also two differences observed between the low speed and high speed maneuvers. First, the low speed front and rear blade minimum shank moments were greater in magnitude than the high speed minimum. This was explained by the fact that the aircraft was pitched up more at low speed flight to obtain enough lift for stabilized flight. Second, the high speed maneuver showed front and rear hyperbolas with larger slopes than the low speed case, highlighting the increased moment sensitivity to yaw angle as aircraft airspeed increased.

A 1P band pass filter was used to obtain a playback of 1P vibratory shank moments for the high and low speed maneuvers. Figures 38 and 39 illustrate the plotted 1P data. Rear blade 1P moments were close to the total moment values for all yaw angles. This suggests that the rear blade response was almost totally 1P. Front blade 1P data showed more differentiation from total moments at the lower yaw angles. The total moments were substantially greater. This difference in total and vibratory data occurred because the front blade experiences a higher portion of 2P response than the rear blade during counter-rotating operation.

A computer program was used to curve fit yaw maneuver data to the equation:

$$M = K \sqrt{\alpha_o^2 + (\psi - \psi_o)^2}$$

- M = Vibratory flatwise shank moment, N-m (ft-lb).
- K = Sensitivity per degree of inflow change, N-m/deg (ft-lb/deg).
- α_o = Pitch offset (vertical offset), or yaw offset in the case of a pitch maneuver, deg.
- ψ = Yaw angle, or pitch angle in the case of a pitch maneuver, deg.
- ψ_o = Yaw offset (horizontal offset) or pitch offset in the case of a pitch maneuver, deg.

Figures 40 and 41 show the resulting curve fit for the low and high speed cases.

The curve fit to low speed data resulted in a sensitivity (K) of 96 N-m/degree (71 ft-lb/deg) for the front and 116 N-M/degree (86 ft-lb/deg) for the rear blades. The low speed pitch offset (α_0) (minimum moment divided by the sensitivity) was calculated as 5.1° for the front and 6.6° for the rear blades. The measured pitch of the lowspeed maneuver was 6°. This substantiates that the above equation correlates well with test data.

The corresponding curve fit to the high speed data resulted in a sensitivity (K) of 148 N-M/degree (109 ft-lb/deg) for the front and 165 N-M/degree (122 ft-lb/deg) for the rear blades. The sensitivity of moment to yaw angle increased with airspeed. The calculated pitch offset was 1.6° for the front and 3.1° for the rear blades. The front blade pitch offset compares reasonably well with the measured pitch angle of 1°. The rear blade pitch offset does not show the same degree of correlation as the front blade. The greater pitch offset of the rear blade was also exhibited during the low speed yaw maneuver, but to a lesser extent. Both yaw maneuvers show little yaw horizontal offset (ψ_0) of the front blade but a substantial horizontal offset of the rear blade, especially at high speed. The yaw offset experienced by the rear blade must be due to the interaction between the front and rear propellers because of counter-rotation.

3.4.3 Pitch Maneuvers

As in the yaw maneuvers, there were two pitch maneuvers (also called roller-coaster maneuvers), one at a low speed 259 Km/hr (140 knts) condition and the other at a high speed 333 Km/hr (180 knt) condition. The pitch maneuver consisted of a pull-up producing a high g loading and a subsequent push-over producing a low g loading. The effective gross weight of the aircraft was changed during this type of maneuver causing a change in aircraft pitch. During high and low speed maneuvers the pitch angle of the propeller axis (boom) always remained positive, meaning at no time did the aircraft achieve a nose down position. Therefore, the pitch data was not as complete as yaw data due to a lack of negative pitch angles. Also, the pitch maneuvers were not smooth transitions as were the yaw maneuvers. This caused the resulting pitch angle and moment data to have more scatter than the yaw maneuver data. Therefore, the pitch results primarily serve the purpose of confirming trends that were established with the yaw maneuvers.

The total vibratory shank moments were plotted versus the pitch angle for high and low speed conditions (see Figures 42 and 43). The plots show half a hyperbolic function in the positive pitch angle range of 0° - 10°.

Some pitch maneuver results can be compared to the yaw maneuvers. Rear blade moments were higher in both cases, and the pitch sensitivity was greater for the high speed maneuver than for the low speed maneuver. This is consistent with the fact that moment sensitivity increases with airspeed.

A 1P band pass filter was also used to play back the pitch maneuvers (see Figures 44 and 45). Both low speed and high speed pitch maneuvers showed the same trends as the 1P yaw maneuvers. The rear blade total and 1P moments were equal suggesting that the rear blade was excited exclusively by 1P excitation. Front blade 1P moments were again significantly lower in magnitude than the total shank moment curves.

Pitch maneuver data was also curve fitted (see Figures 46 and 47) to extract information about the moment sensitivity (K), yaw offset (α_0), and pitch offset (ψ_0) that could not be obtained by visual inspection of the data because of the limited pitch range and scatter in the data. The same equation was used with the pitch data as with the yaw data, but much more error was introduced in the curve fit. Only the trends in the results were applicable for direct comparison to the yaw results. A comparison of the pitch results to the yaw results, Figures 40 and 41 to Figures 46 and 47 show the following similarities. The moment sensitivity per degree of angular inflow for the high speed case was greater than at low speed, and the rear blade response showed a similar horizontal inflow offset (ψ_0) as occurred with aircraft yaw.

3.4.4 Campbell Plots

Campbell plots were constructed from beam analyses for the front and rear propellers. Spectral data obtained during ground running and stabilized flight testing was reduced and analyzed. The spectral analysis did not clearly identify blade natural frequencies. Natural blade modes were not excited to high stress levels, and the spectral plots revealed noise spikes at low level stresses masking the natural blade response. The data points that were plotted were selected on the basis of repeatability of peaks on different strain gages. Although the frequency data was sparse some comparison of the measured modal frequencies with the predicted values was obtained. Figures 48 and 49 illustrate the results of the spectral data reduction superimposed on predicted Campbell plots for the front and rear blades. The torsion mode was predicted very successfully when compared with spectral data. Spectral data showed a torsional critical speed on both blade shear gages at an interblade forcing frequency of 4P front added to 4P rear. While the front and rear propellers were rotating at 1330 and 1070 RPM respectively the excitation frequency was 160 Hz which was the rear blade torsional frequency. Figure 50 is a visicorder playback at these conditions illustrating the 4P plus 4P forced response of the rear blade at the torsional frequency shear gage 14v(R). Note the very low response of the front blade shear gage 14v(F).

Modes 1-4 static frequency prediction was also substantiated well at static conditions when a propeller, either front or rear, was feathered during single-rotation flight test. The bending mode results during blade rotation were not clear. Figures 48 and 49 show scattered results obtained from the

data. Only blade P-order frequencies were prevalent. The blade did not respond well in its natural modes during flight or ground operation. Therefore, the rotating natural frequencies were not substantiated well for this installation so analytical predictions were based on blade models that could not be completely verified. The blade models appeared to be quite satisfactory for all conditions where correlation to data could be made.

3.5 Analytical Predictions

3.5.1 Conditions Examined

Analytical predictions of the blade stresses were made for the Gannet propellers for the comparison with the measured data to verify existing counter-rotation methodology. The calculations were performed using two procedures that will be reviewed in the following discussions. The first calculation procedure used a consistent set of pitch and yaw angles for both counter and single-rotation predictions. This consistent set of angles allowed a direct comparison between single and counter-rotation analytical results. The pitch and yaw angles for this comparison were established from the counter-rotation test conditions shown in Table VIII. The Gannet aircraft was modeled in a flow-field analysis, and the pitch and yaw angles were calculated. A comparison between the experimental and calculated angles is also shown in Table VIII. It should be noted that the aircraft was shown by analysis to induce a 0.4 degree yaw at the boom where pitch and yaw measurements were taken. This error was accounted for in the calculations by reducing the measured yaw angle. The comparison was generally good for the modeled configuration over the range of airspeed from 222 to 370 Km/hr (120 to 200 knts). The corresponding single-rotation test conditions showed somewhat higher measured angles than the counter-rotation test conditions even though the test pilot attempted to match the single and counter-rotation conditions for comparison purposes.

Once the aircraft flow-field was established, the effect of the propeller was superimposed on the aircraft flow field so the harmonic blade loads could be calculated for subsequent stress predictions. The superposition of the aircraft flow-field on the propeller induced flow accounted for the effects of single or counter-rotation for the subsequent response calculations. Six load calculations were performed to cover the analytical comparison of single to counter-rotation and the comparison of analysis to test data. The cases compared are summarized in Table IX for combinations of high airspeed, low airspeed, single rotation, and counter-rotation. The blade response for these six cases were determined by combining the harmonic blade loads with the blade structure using a modal response analysis program. The response analysis used for this study was a beam analysis that was limited to bending modes. Therefore the 8P response of the blades in torsion was not modeled.

3.5.2 Counter-Rotation Analysis

The calculated blade response was dominated by the 1P harmonic as occurred with the test data. Figures 51 and 52 show the comparison of the counter-rotation 1P predictions to the test data. Overall the agreement was good considering the low level of measured blade stress except at the inboard bending gage, 50.8 cm (20 in.) station, where a rather large discrepancy exists between the test data and analytical predictions for the rear propeller. The difference between measurement and calculation at the 50.8 cm (20 in.) station was inconsistent with the results at the blade shank and mid-blade regions. This discrepancy could not be resolved with the available information.

3.5.3 Counter-Rotation vs Single-Rotation

Figures 53 through 56 show a comparison of counter-rotation predictions to single-rotation predictions. The analytical predictions showed that counter-rotation always had an adverse effect on the 1P stressing of the propeller and that the adverse effect was evident on both the front and rear blade rows. At low speed the predictions showed that counter-rotation increased the stresses on the front blade slightly more than the rear blade because of the influence of induced flow from the rear blade on the front blades. At high speed the analysis showed that the rear blade was strongly affected by counter-rotation while the front blade was affected only to a small degree. These results are somewhat contrary to the conclusions drawn from the experimental results in section 3.4 where the test data showed that the front blade was unaffected by counter-rotation at both high and low speed conditions and that the rear blade was adversely affected by counter-rotation at both high and low speed conditions. A summary of the comparison between the analysis and test data is given in Table X for blade shank bending moments. The summary is in terms of absolute values and ratios of the results. It is evident from the table that the sensitivity of the high speed results causes poor correlation whereas the low speed results generally show good correlation.

These differences at high speed were in part due to the sensitivity of the analysis to discrepancies in pitch and yaw angle. The magnitude of the measured and calculated stresses at high speed were small. Therefore a slight difference in angular inflow will result in a poor comparison of test to analysis. In addition, the values of the measured stresses were small and may be subject to a relatively large experimental error. The comparison of analysis to test data, particularly at high speed, was more of a comparison of one small number to another small number, and therefore was not a good check on the ability of the analysis to predict experimental results.

3.5.4 Single-Rotation Analysis

To illustrate the sensitivity of the analysis to pitch and yaw angles a second calculation procedure was utilized to make predictions for single-rotation operation using the measured inflow angles shown in Table XI. These results are shown in Figures 57 through 60. When the measured angles were used in the analysis the agreement between test and calculation was better over the entire blade for both front and rear propellers. A comparison of the high speed results shown in Figures 59 and 60 with the previous high speed single-rotation results from figures 55 and 56 shows the sensitivity of the predicted stress to inflow angle at high speed flight conditions. This sensitivity was also displayed in the 259 Km/hr (140 knt) and 333 Km/hr (180 knt) yaw and pitch maneuver data in Section 3.4.

4.0 CONCLUSIONS

The results from the flight stress survey on the Fairey Gannet aircraft have shown that counter-rotation can have a significant effect on the response of a propeller to angular inflow. The stabilized flight data showed that the once-per-revolution (1P) forced excitation on the rear propeller of a counter-rotating installation was adversely affected by the influence of the front propeller. The front propeller was not significantly affected by the rear propeller. Counter-rotation increased the flatwise blade vibratory shank bending moment of the rear propeller by approximately 25% over the same propeller operating in a single-rotation configuration.

For this installation the response at harmonics higher than 1P was not significant. However, the higher order response of the front and rear propellers was generally greater for counter-rotation operation than for single-rotation operation. The blade passage frequency excitation of the counter-rotating propeller was evident in the data but the resulting stress and moment levels were low. The only case where significant blade passage excitation was evident occurred during mis-matched propeller RPM operation on the ground when a critical speed was encountered. If the critical speeds associated with the blade passage excitation were avoided, no significant response was evident. The yaw and pitch maneuver data also showed the effects of counter-rotation. The resulting response of the rear blade to a yaw maneuver indicated that the front propeller imparted an inflow that had the effect of a built-in inflow angle on the rear propeller. In other words, the rear propeller was not at the lowest level of response at zero degrees inflow angle while the front propeller was essentially at the lowest response at zero inflow angle.

The methodology used to calculate the response of the Fairey Gannet counter-rotating propeller showed a varying degree of correlation with the test data. The correlation at low speed flight was generally good. The counter-rotating predictions showed an increased stress over single-rotation operation. However the analysis did not show the rear propeller response increase to the extent that was established from test results. There were discrepancies in correlation between analysis and test at high speed due to the sensitivity of the high speed results to small changes in inflow angle and the relatively small values of measured stress. Therefore, the high speed results were not a good check of the methodology.

Overall the test results from the Fairey Gannet aircraft will be useful in refining the methodology required to predict the aerodynamic interaction between the propellers of counter-rotating installations. The interaction effects that were displayed in the flight data were produced by the same aerodynamic loads that affect propeller noise and performance. Therefore, the use of this data to refine future response analyses will result in the improvement of noise and performance calculation.

5.0 Recommendations

Results from the Fairey Gannet Aircraft structural tests revealed a number of presently unknown and unpredicted characteristics concerning the response of a counter-rotating propeller in angular inflow. These results point out areas of study required to advance the present state-of-the-art counter-rotating propeller technology. Both the empirical data base and analytical methodologies for counter-rotating structural response studies are in need of enhancement.

The empirical data base should be expanded initially in the model scale with a controlled wind tunnel environment to Mach numbers up to 0.8. Structural testing of the CRP-X1 counter-rotating Prop-Fan model is being performed by Hamilton Standard to provide an expanded data base for counter-rotating analysis methodology. In addition to the structural response data, further efforts should be expended to measure the flow field encountered by both the front and rear stages of a counter-rotating propeller or Prop-Fan.

Direct measurements of the flow environment under wind tunnel conditions would be useful for confirming counter-rotating aerodynamic analyses. Without flow field measurements the aerodynamic analyses are confirmed from secondary results of performance and structural response.

In addition to the expansion of the empirical data base the counter-rotation analytical methods need re-evaluation because of the differences displayed between predicted and measured response on the Gannet propellers. Deficiencies in the present methodology should be identified and rectified. Also, new analytical methods should be identified or developed for future counter-rotating structural analysis.

6.0 References

1.0 Weisbrich, A.L., Godston, J. and Bradley, E.: Technology and Benefits of Aircraft Counter-Rotation Propellers, NASA CR-168258, December, 1982.

**TABLE I FAIREY GANNET FRONT PROPELLER BLADE
BEAM PROPERTIES**

Station	Radius	Area	I-Minor	I-Major	I-Polar	Radius of Gyration
	cm	cm ²	cm ⁴	cm ⁴	cm ⁴	cm ²
1	16.51	154.4	2149.	2149.	4296	27.83
2	20.32	127.5	1704.	1704.	3409.	26.74
3	22.86	153.7	2582.	2582.	5165.	33.60
4	27.94	117.8	617.7	1999.	2617.	22.21
5	33.02	104.	332.1	2223	2555	24.56
6	38.10	96.84	228.6	2450	2678.	27.66
7	50.80	83.68	113.8	2789.	2903.	34.69
8	63.50	77.35	77.54	2822.	3045.	38.08
9	78.74	61.65	39.36	2437.	2621.	40.90
10	88.90	56.91	31.98	2267.	2441	41.17
11	104.1	47.15	17.95	1853.	2005	40.57
12	114.3	40.66	11.88	1548.	1690.	39.39
13	129.5	33.74	7.34	1165.	1289.	35.87
14	139.70	33.02	5.60	942.3	1051.	32.71
15	154.9	20.54	2.25	487.	563.	25.07
16	165.1	14.80	1.06	257.	307.7	18.68
17	177.8	8.7	.32	82.54	107.4	10.78
18	185.4	6.4	.19	34.07	46.8	6.27
19	190.5	.60	.0003	.09	.192	.37

TABLE II FAIREY GANNET REAR PROPELLER BLADE
BEAM PROPERTIES

Station	Radius	Area	I-Minor	I-Major	I-Polar	Radius of Gyration
	cm	cm ²	cm ⁴	cm ⁴	cm ⁴	cm ²
1	20.32	154.4	2149	2149	4296	27.83
2	22.86	127.5	1704	1704	3409	26.74
3	25.40	98.00	1211	1211	2423	24.73
4	27.94	119.81	812.5	1620	2432	20.30
5	33.02	79.81	222.8	1101.	1324.	16.59
6	38.10	72.77	140.7	1270	1411	19.38
7	50.80	67.48	74.05	1812	1886	27.96
8	63.50	63.12	44.62	2171	2344	35.74
9	78.74	54.70	28.02	2201	2369	41.57
10	88.90	49.32	19.91	2040	2199	42.66
11	104.1	41.44	11.82	1685	1833	42.01
12	114.3	36.56	8.4	1407	1553	39.92
13	129.5	29.05	4.61	997.3	1117	35.74
14	139.70	26.74	3.96	829.1	931.1	32.37
15	154.9	16.97	1.29	379.6	447.4	23.82
16	165.1	12.89	.86	215.6	263.8	18.44
17	177.8	7.38	.20	63.81	85.33	9.98
18	185.4	2.81	.02	7.15	11.11	3.35
19	190.5	.65	.0005	.11	.22	.37

TABLE III. COMPARISON OF MEASURED AND PREDICTED MODAL FREQUENCIES FOR THE FAIREY GANNET PROPELLER BLADES.

Mode	Modal Frequency, Hz			
	Front Blade		Rear Blade	
	Measured	Predicted	Measured	Predicted
1st flatwise	19.8	19.73	17.3	17.6
2nd flatwise	51.9	51.90	49.5	49.5
1st edgewise	—	79.14	—	78.5
3rd flatwise	—	125.83	113.4	115.7
1st torsion	178.9	183.89	163.2	160.8

TABLE IV FAIREY GANNET STRAIN GAGE INSTALLATION

Gage Number*	Gage Location			
1SFF	Shank	flatwise	front row	blade 1
2SFF	Shank	flatwise	front row	blade 2
1SEF	Shank	edgewise	front row	blade 1
2SEF	Shank	edgewise	front row	blade 2
1SFR	Shank	flatwise	rear row	blade 1
2SFR	Shank	flatwise	rear row	blade 2
1SER	Shank	edgewise	rear row	blade 1
2SER	Shank	edgewise	rear row	blade 2
11F	Front row	50.8 cm	station bending at the 50% chord	
11R	Rear row	50.8 cm	station bending at the 50% chord	
12F	Front row	129.5 cm	station bending at the 50% chord	
12R	Rear row	129.5 cm	station bending at the 50% chord	
13F	Front row	160 cm	station bending at the 50% chord	
13R	Rear row	160 cm	station bending at the 50% chord	
14VF	Front row	129.5 cm	station Vee at the 50% chord	
14VR	Rear row	129.5 cm	station Vee at the 50% chord	
Note:	<p>Shank gages are applied in push-pull pairs, as shown in the Figures 9 and 10 on the circular blade station outboard of the serrated region. This is about the 22.9 cm station for the front blade and about the 25.4 cm station for the rear blade.</p> <p>All other gages are installed on the camber side of blade 1. Bending gages are aligned radially and vee gages are push-pull pairs aligned $\pm 45^\circ$ from radial.</p> <p>The shank gages on each blade row are to be calibrated against known loads to determine moment/strain relationships.</p> <p>* Blades 1 and 2 are any adjacent blades in a blade row.</p>			

TABLE V STABILIZED FLIGHT TEST CONDITIONS

Run No.	% Power		% RPM		Indicated Airspeed Km/hr	Altitude ~ m	
	Front	Rear	Front	Rear		Start	Finish
1	80	80	99.5	100	222	2896	3505
2	80	82	99.5	100	259	2896	3353
3	80	82	99.5	100	259	2896	3200
4	40	82	99.5	100	259	2896	3078
5	80	30	99.5	100	259	2896	3048
6	82	84	99.5	100	296	2885	2957
7	82	84	99.5	100	333	3048	3170
8	83	85	99.6	100	370	3139	3048
9	80	—	99.8	—	222	3078	3018
10	78	—	99.3	—	259	3200	3200
11	78	—	99.4	—	296	3170	3018
12	80	—	99.6	—	333	3139	2774
13	—	80	—	100	222	3048	3109
14	—	80	—	100	259	3048	3018
15	—	82	—	100	296	3078	2896
16	—	83	—	100	333	3231	3018
17	—	83	—	100.5	370	3353	3018
18	82	—	99.7	—	370	3353	2987

100% Power = 1380 Kw (1850 SHP)

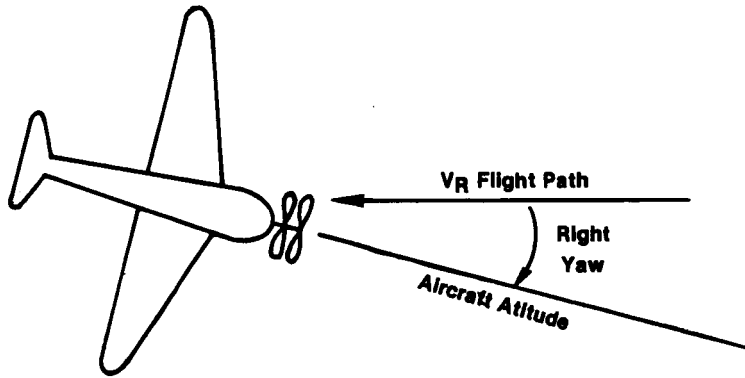
100% RPM = 1310 RPM

TABLE VI ROLLER COASTER FLIGHT MANEUVER TEST CONDITIONS

Run No.	% Power		% RPM		Airspeed Km/hr	Altitude ~ m		Maneuver
	Front	Rear	Front	Rear		Start	Finish	
19A	80	84	99.5	100	259	2743		Level
19B	↓	↓	↓	↓	259			Pull-up
19C	↓	↓	↓	↓	259			Level
19D	↓	↓	↓	↓	259			Pushover
19E	80	84	99.5	100	259			3810
20A	82	84	99.5	100	333	3048		Level
20B	↓	↓	↓	↓	333			Pull-up
20C	↓	↓	↓	↓	333			Level
20D	↓	↓	↓	↓	333			Pushover
20E	82	84	99.5	100	333			3414

TABLE VII SIDE SLIP FLIGHT MANEUVER TEST CONDITIONS

Run No.	% Power		% RPM		Indicated Airspeed Km/hr	Altitude~m		Maneuver
	Front	Rear	Front	Rear		Start	Finish	
21A	82	83	99.5	100	259	2743		Center
21B	82	83	99.5	100	259			Yaw Left
21C	82	83	99.5	100	259			Yaw Right
21D	82	83	99.5	100	259		3840	Center
22A	83	84	99.5	100	333	3048		Center
22B	83	84	99.5	100	333			Yaw Left
22C	83	84	99.5	100	333			Yaw Right
22D	83	84	99.5	100	333		3292	Center



**TABLE VIII MEASURED AND CALCULATED YAW AND PITCH ANGLES
FOR THE FAIREY GANNET AIRCRAFT DURING
COUNTER-ROTATING OPERATION**

Run Number	Airspeed Km/hr	Measured		Calculated	
		Pitch Deg.	Yaw Deg.	Pitch Deg.	Yaw* Deg.
1	222	8	.5	8.4	.1
2	259	6.5	0	4.8	-.4
6	296	3	.5	2.6	.1
7	333	1	1.0	1.1	.6
8	370	0	1.5	.05	1.1

* Calculated yaw angles are the measured results minus the calculated .4 degree induced angle at the boom.

TABLE IX SUMMARY OF CALCULATED TEST CASES

Case	Airspeed km/hr	Mode of operation
1	222	Counter rotating
2	222	Single rotation front
3	222	Single rotation rear
4	370	Counter rotating
5	370	Single rotation front
6	370	Single rotation rear

TABLE X COMPARISON OF MEASURED AND CALCULATED IP SHANK BENDING MOMENTS FOR THE GANNET AIRCRAFT DURING COUNTER AND SINGLE ROTATION OPERATION

Airspeed Km/hr	Blade row	Mode of operation	Measured		Calculated		Comparison
			Moment N-m	Ratio CR/SR	Moment N-m	Ratio CR/SR	<u>Measured</u> <u>Calculated</u>
Low speed 222 Km/hr	Rear	Single rotation	791	1.29	914	1.08	0.87
		Counter rotation	1017		988		1.03
	Front	Single rotation	678	1.08	905	1.18	0.75
		Counter rotation	734		1068		0.69
High speed 370 Km/hr	Rear	Single rotation	452	1.25	246	1.61	1.84
		Counter rotation	565		396		1.43
	Front	Single rotation	226	1.0	238	1.20	0.95
		Counter rotation	226		285		0.79

TABLE XI MEASURED PITCH AND YAW ANGLES FOR THE FAIREY GANNET DURING SINGLE-ROTATION OPERATION

Run Number	Airspeed Km/hr	Propeller Operating	Pitch Deg.	Yaw Deg.
13	222	Front	9	1
14	259	Front	7	.5
15	296	Front	3	.5
16	333	Front	1	.5
17	370	Front	0	1.5
9	222	Rear	9	1
10	259	Rear	7	1
11	296	Rear	3	1
12	333	Rear	1	2.5
18	370	Rear	0	2

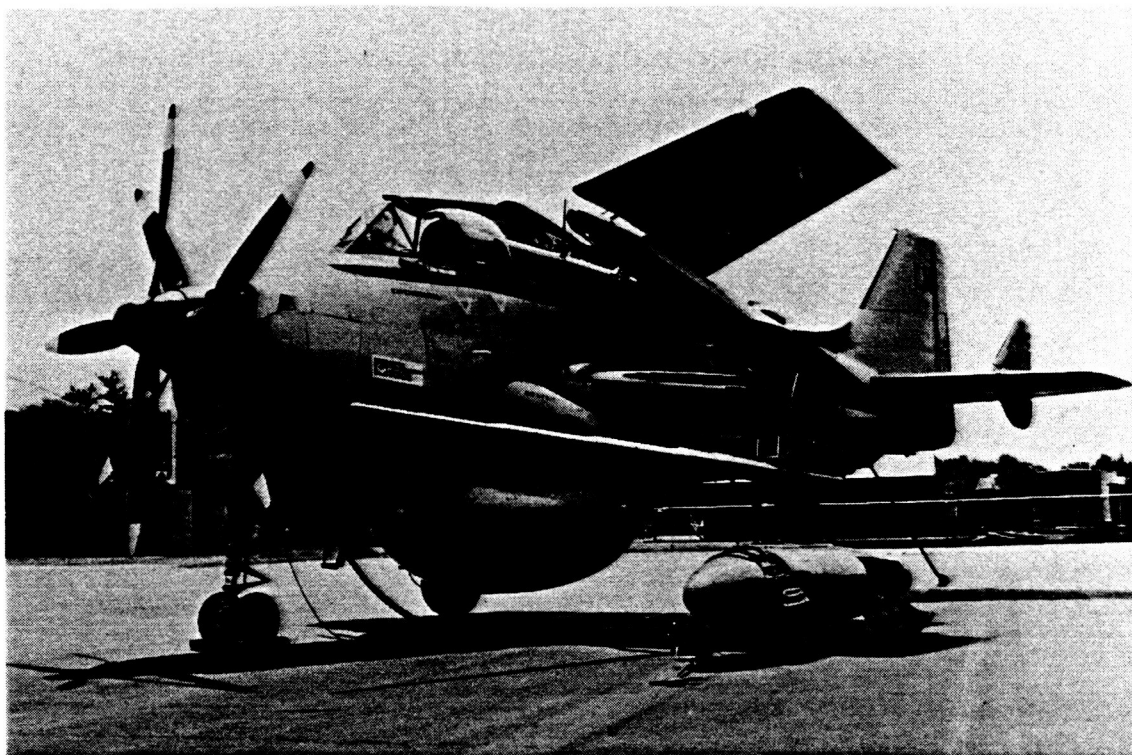


FIGURE 1. FAIREY GANNET AIRCRAFT

ORIGINAL PAGE
BLACK AND WHITE PHOTOGRAPH

~~ORIGINAL PAGE
COLOR PHOTOGRAPH~~

NASA CR 174819



FIGURE 2. FAIREY GANNET AIRCRAFT WITH ACOUSTIC TEST BOOM

ORIGINAL PAGE
BLACK AND WHITE PHOTOGRAPH

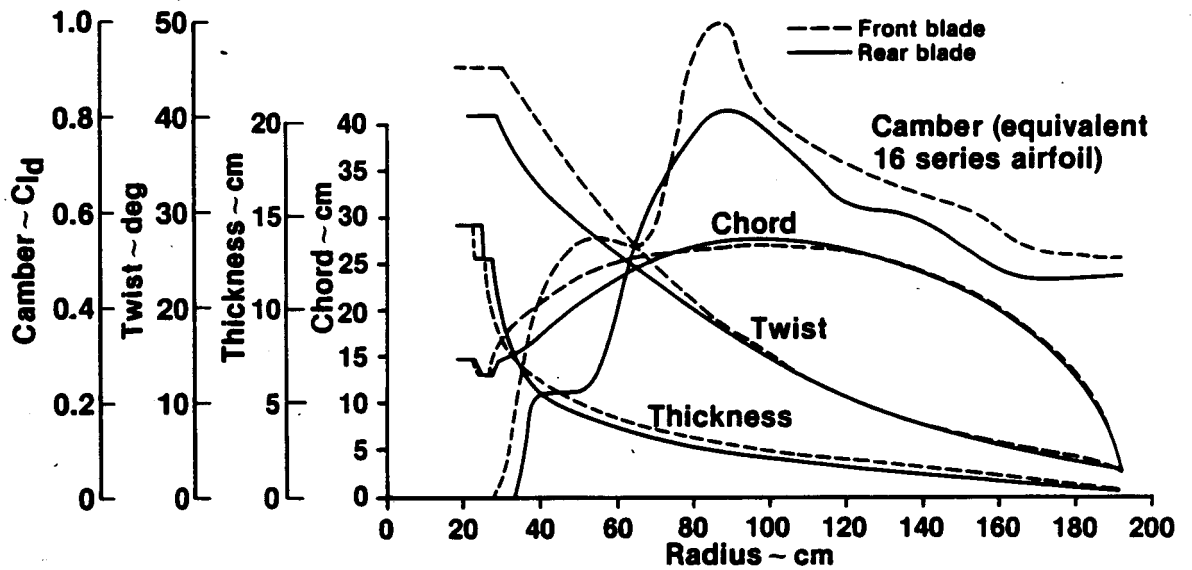
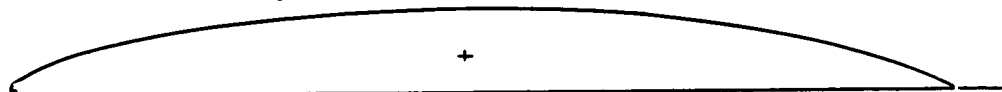


FIGURE 3. FAIREY GANNET PROPELLER BLADE GEOMETRY

Camber

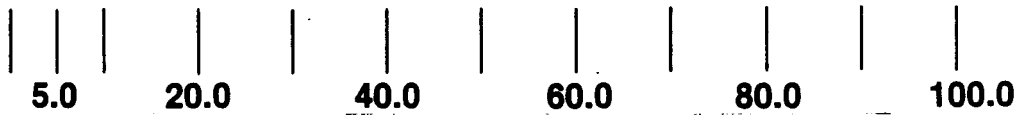
Equivalent 16 Series Airfoil



Measured Section



Face



Distance from leading edge, percent chord

FIGURE 4. MEASURED AIRFOIL SECTION VS. SERIES 16 AIRFOIL FOR THE FAIREY GANNET REAR BLADE, 88.9 CM STATION

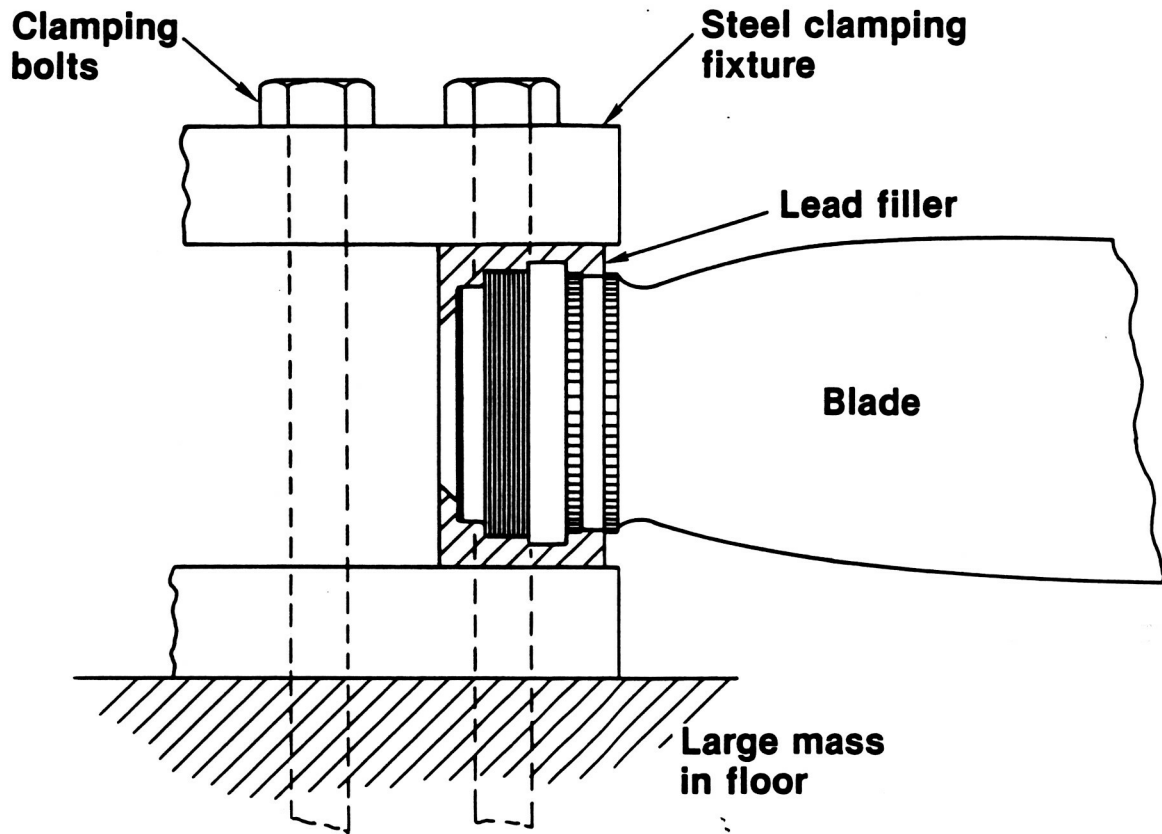


FIGURE 5. FREQUENCY TEST SET-UP

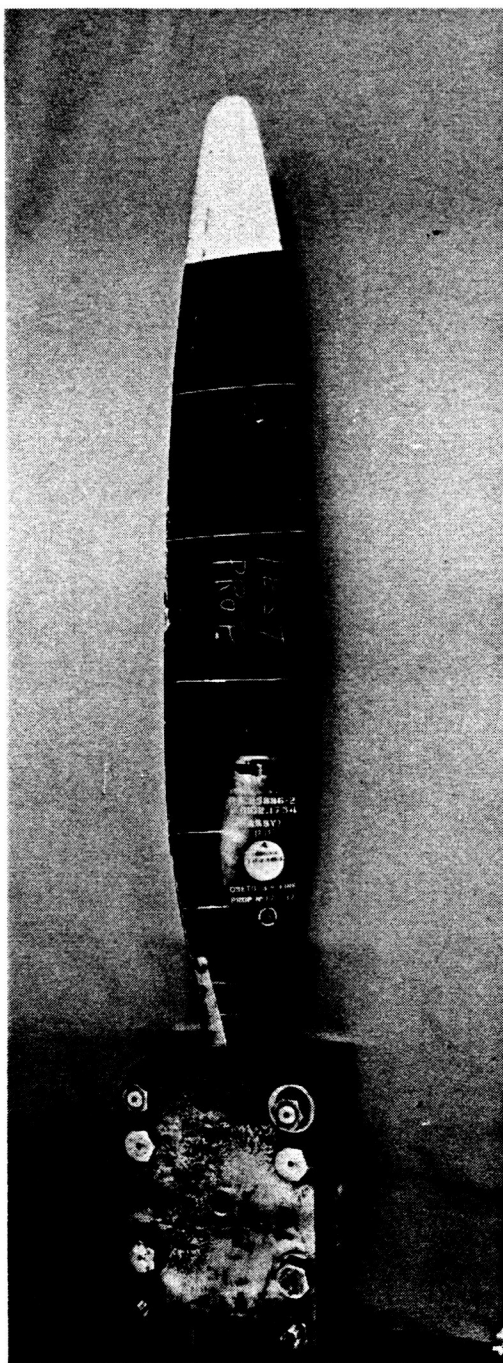


FIGURE 6. GANNET REAR BLADE FREQUENCY TEST SET-UP

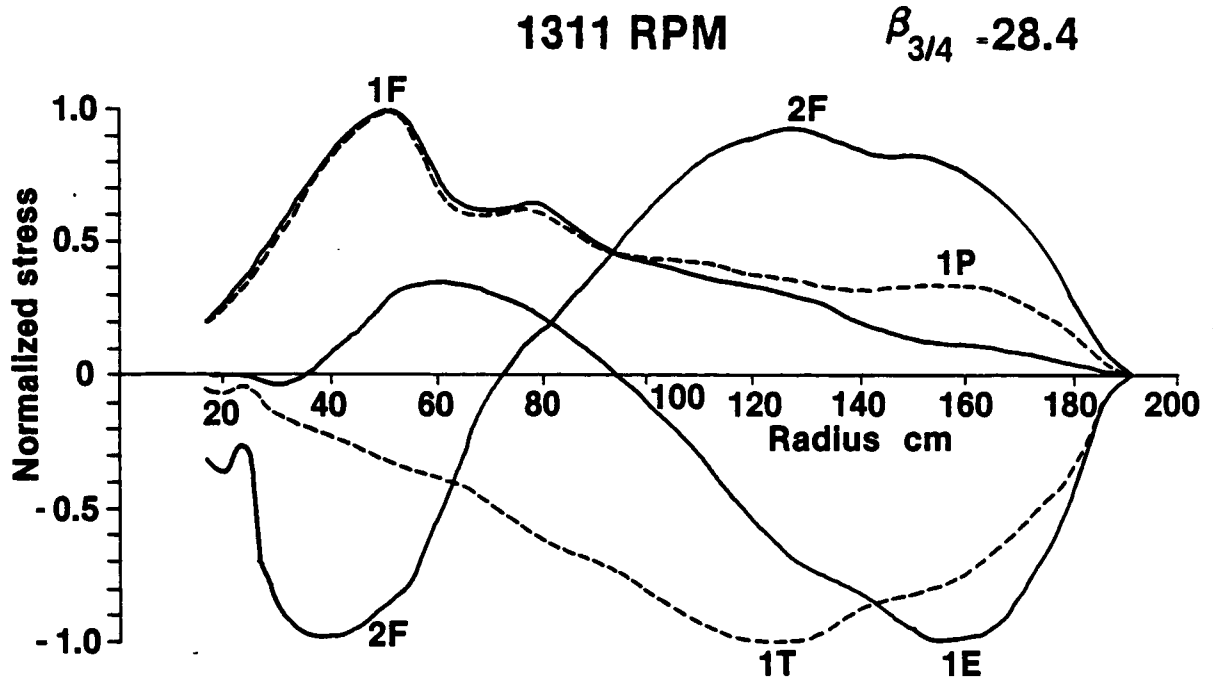


FIGURE 7. PRELIMINARY FLATWISE STRESS DISTRIBUTIONS FOR THE GANNET FRONT BLADE.

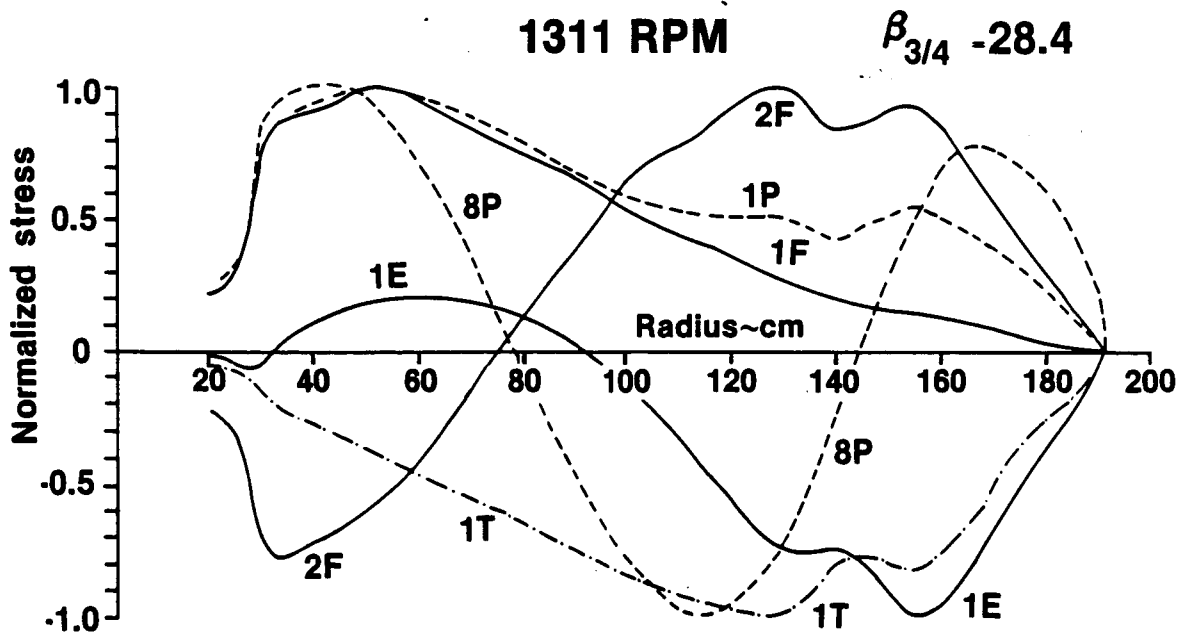


FIGURE 8. PRELIMINARY FLATWISE STRESS DISTRIBUTIONS FOR THE GANNET REAR BLADE

Shank gage locations
 Root to tip view angles
 referenced to $\frac{3}{4}$ radius station

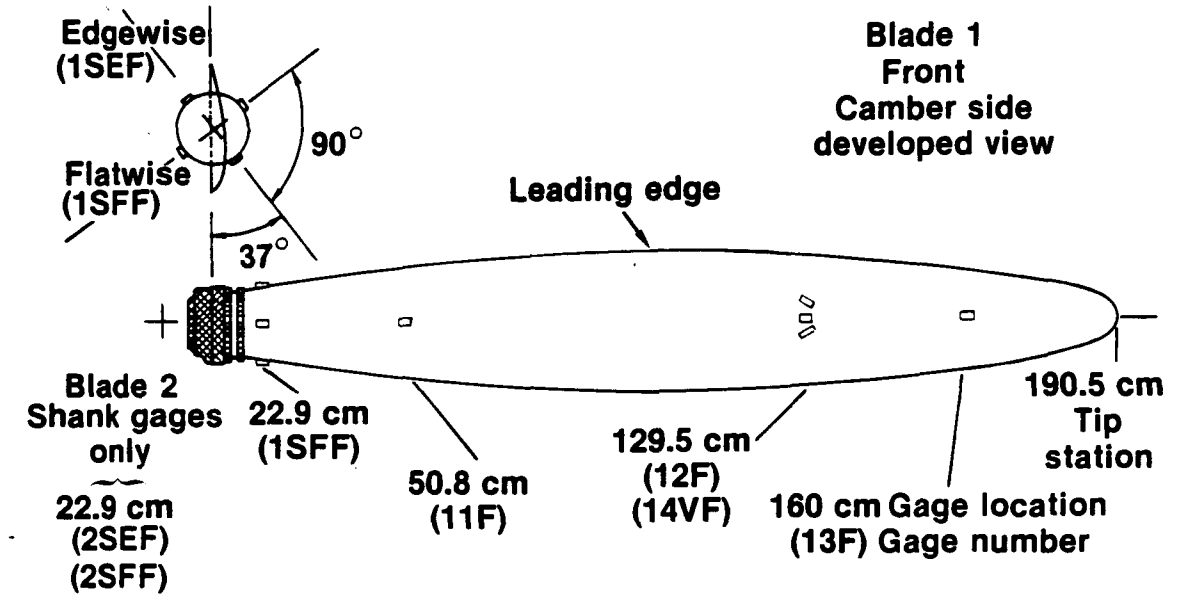


FIGURE 9. FAIREY GANNET PROPELLER FRONT BLADE STRAIN GAGE LOCATIONS

Shank gage locations
 Root to tip view angles
 referenced to $\frac{3}{4}$ radius station

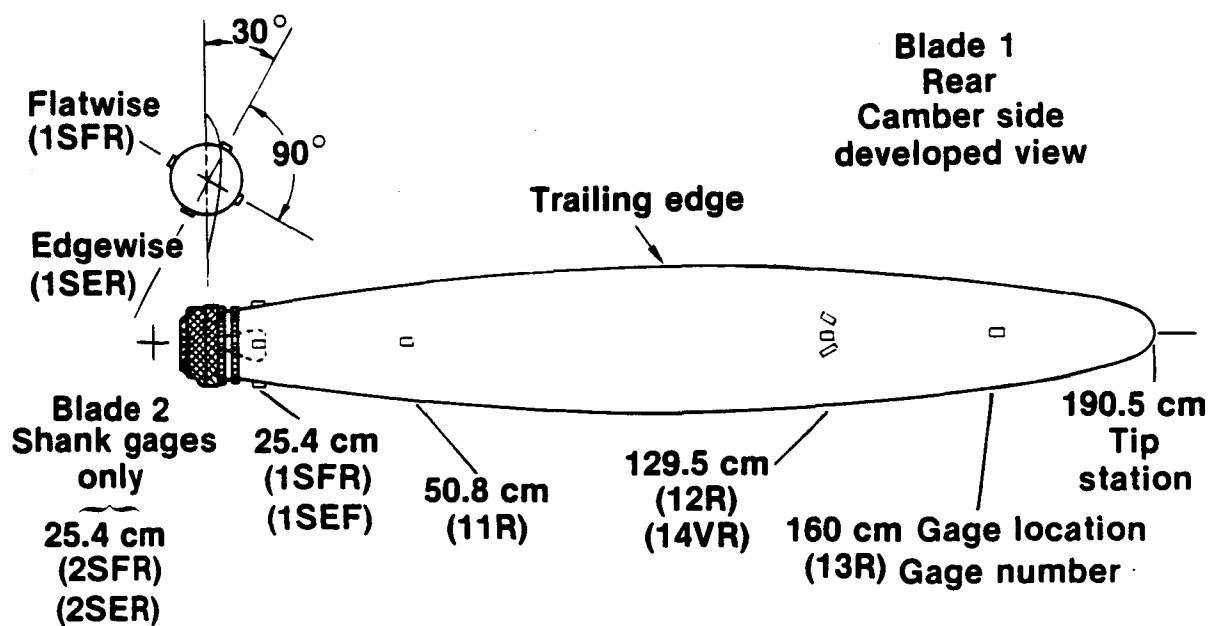


FIGURE 10. FAIREY GANNET PROPELLER REAR BLADE STRAIN GAGE LOCATIONS

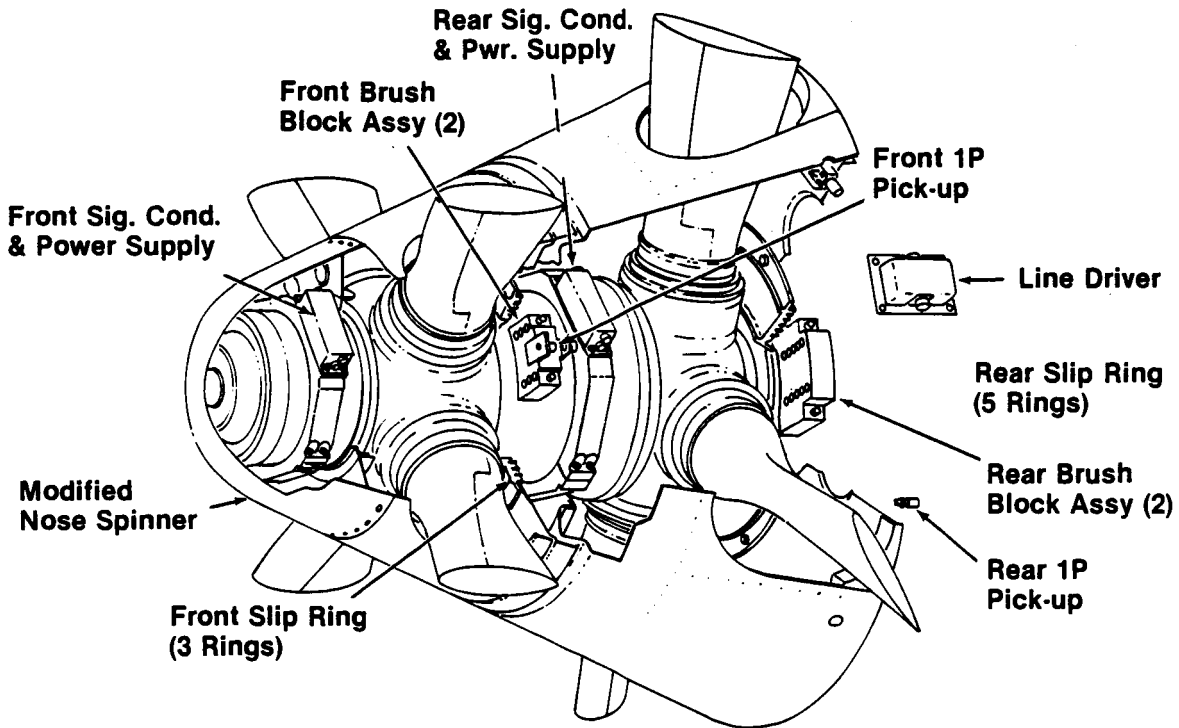


FIGURE 11. FAIREY GANNET FM SYSTEM INSTALLATION

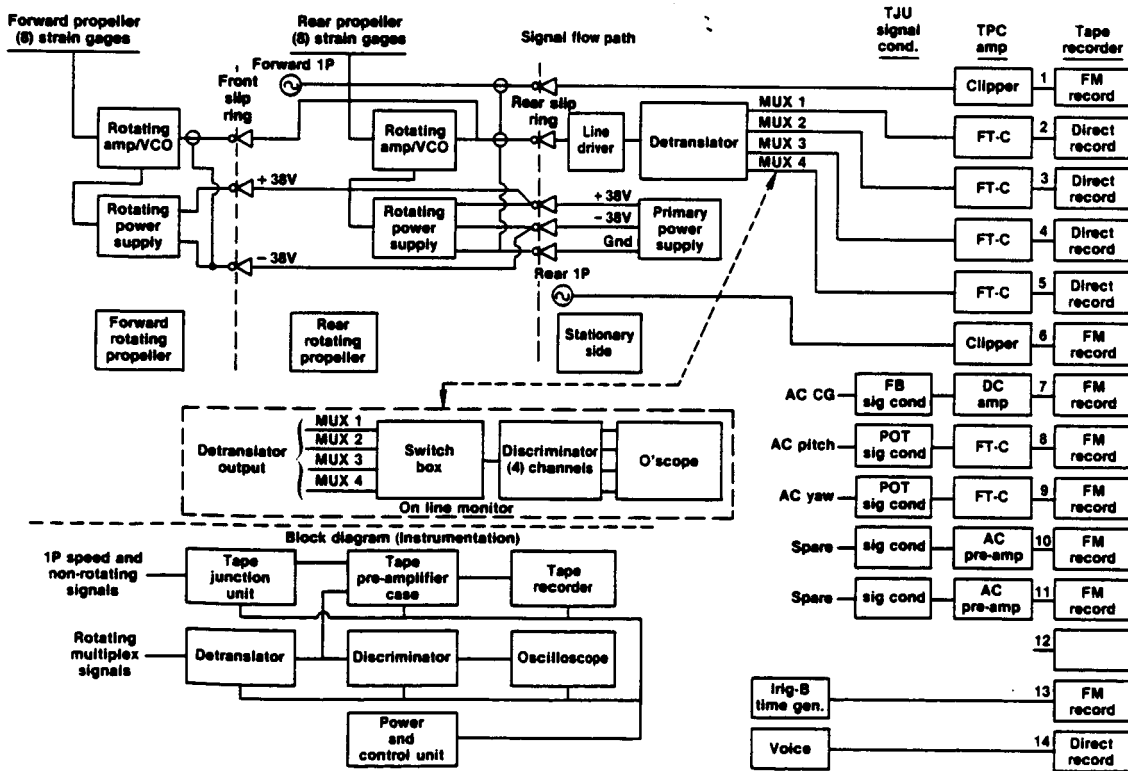


FIGURE 12. FAIREY GANNET INSTRUMENTATION

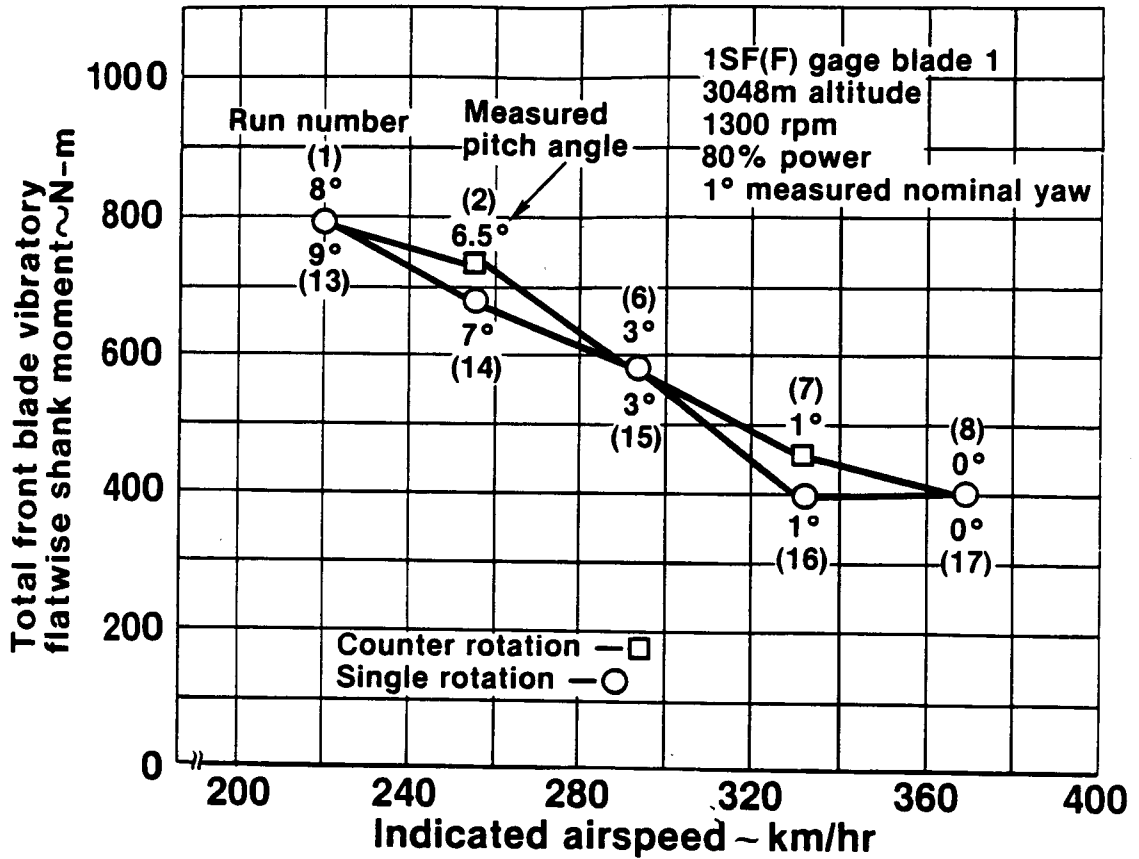


FIGURE 13. GANNET STABILIZED FLIGHT FRONT BLADE 1 FLATWISE TOTAL VIBRATORY SHANK MOMENT COMPARISON

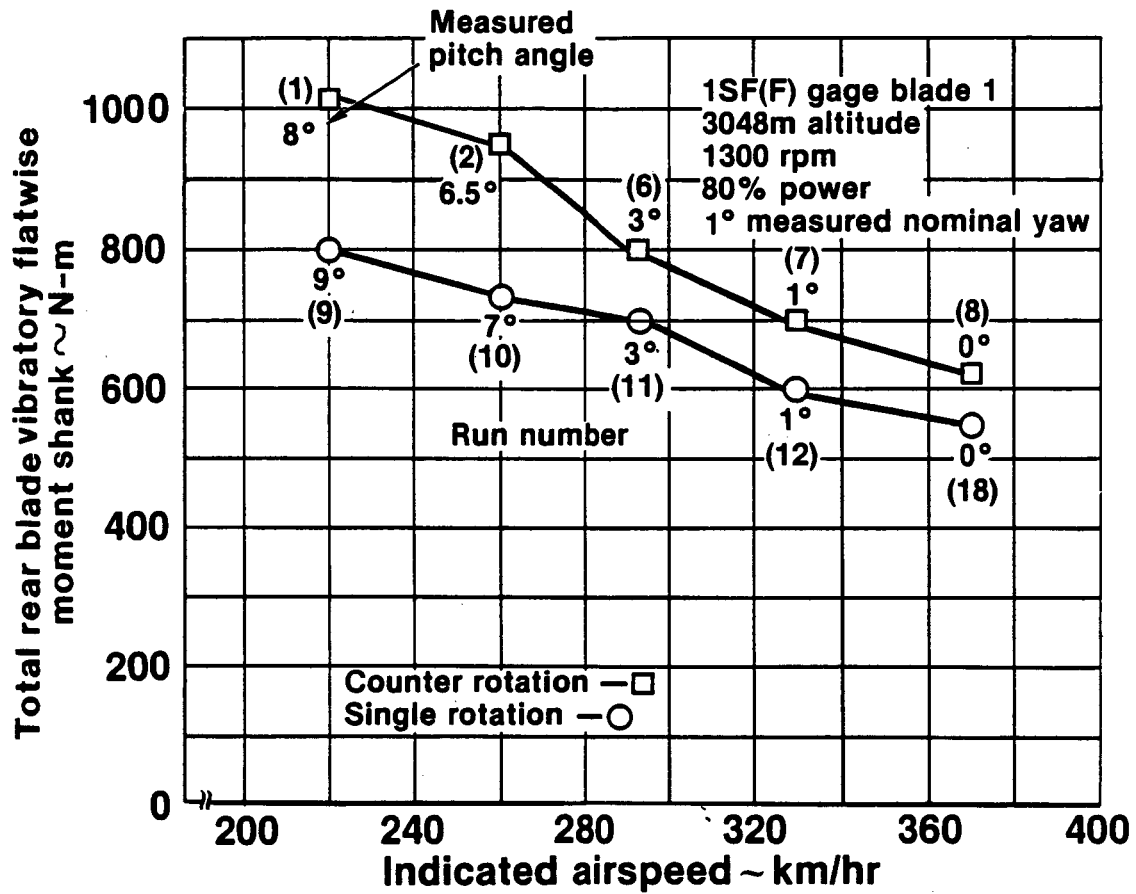


FIGURE 14. GANNET STABILIZED FLIGHT REAR BLADE 1 FLATWISE TOTAL VIBRATORY SHANK MOMENT COMPARISON

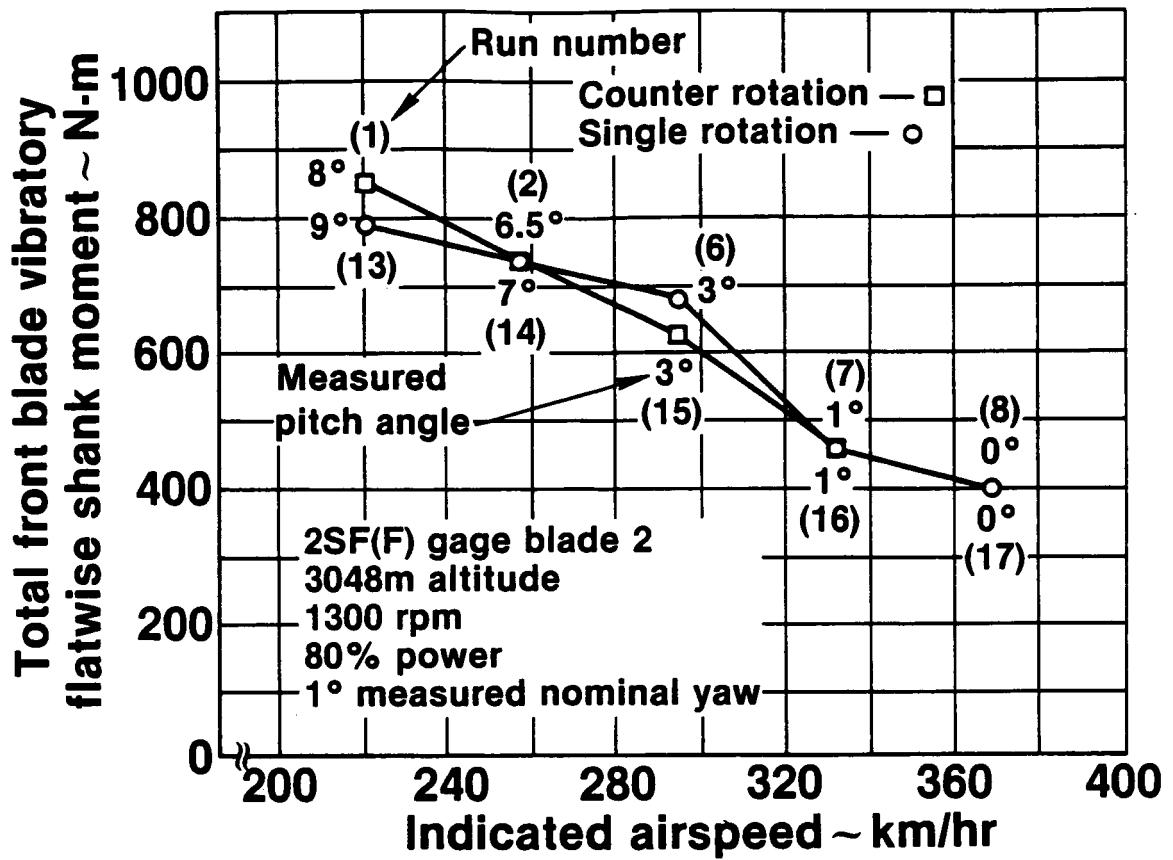


FIGURE 15. GANNET STABILIZED FLIGHT FRONT BLADE 2 FLATWISE TOTAL VIBRATORY SHANK MOMENT COMPARISON

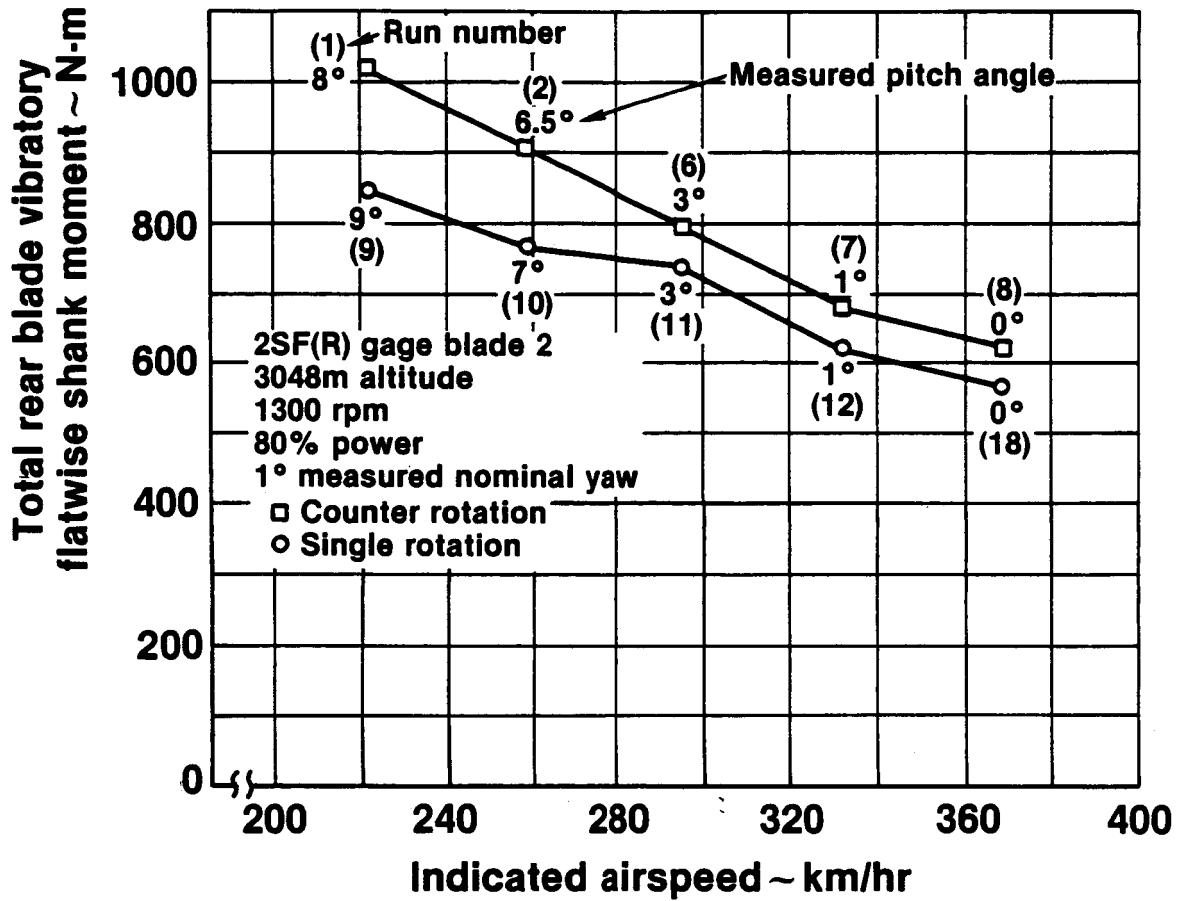


FIGURE 16. GANNET STABILIZED FLIGHT REAR BLADE 2 FLATWISE TOTAL VIBRATORY SHANK MOMENT COMPARISON

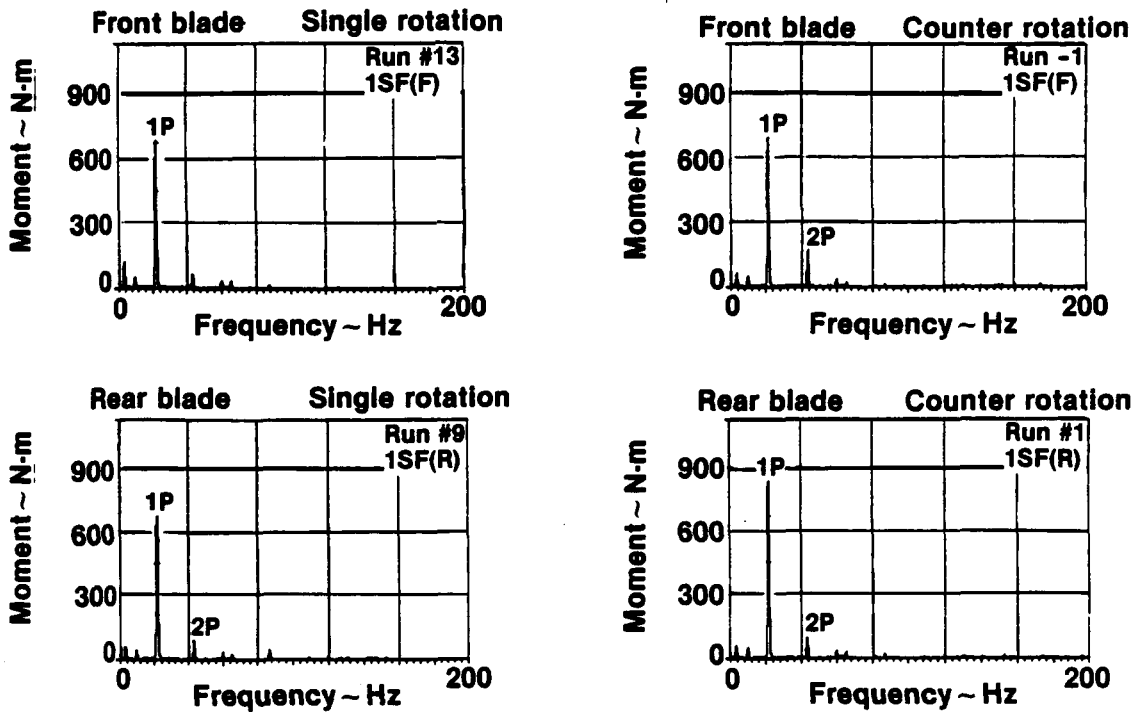


FIGURE 17. FLATWISE SHANK BENDING MOMENT COMPONENTS FOR GANNET LOW SPEED FLIGHT 222 KM/HR

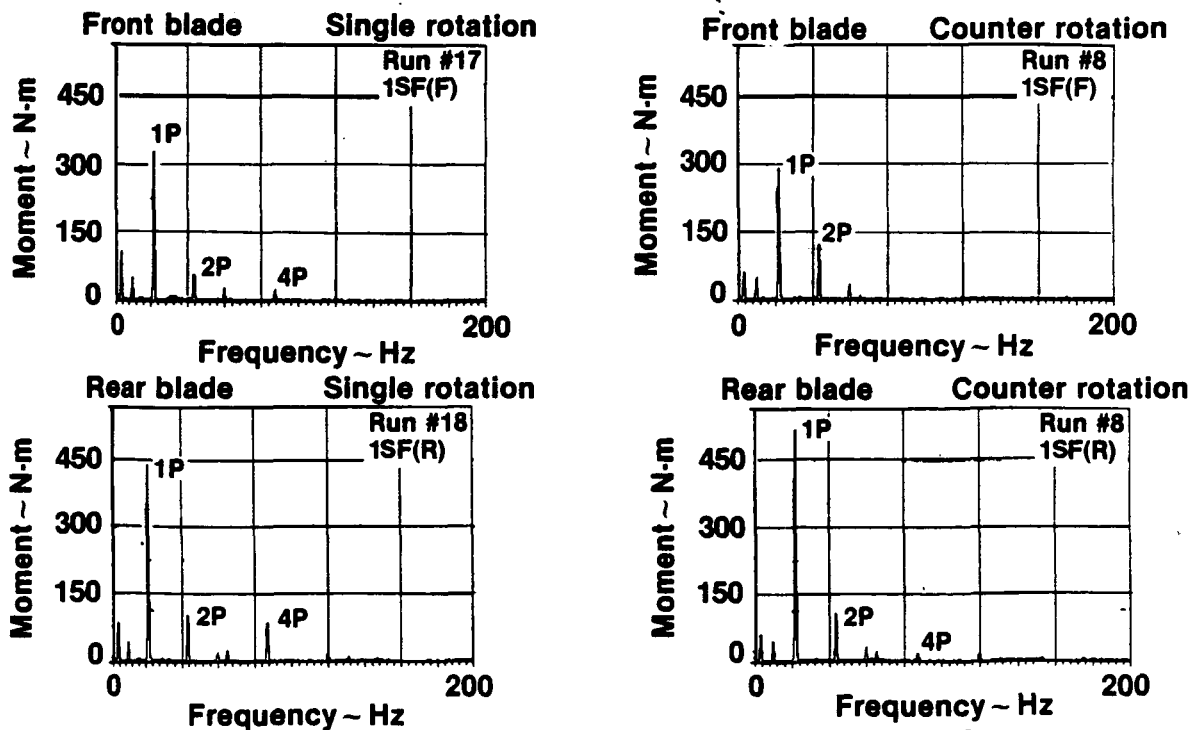


FIGURE 18. FLATWISE SHANK BENDING MOMENT COMPONENTS FOR GANNET HIGH SPEED FLIGHT 370 KM/HR

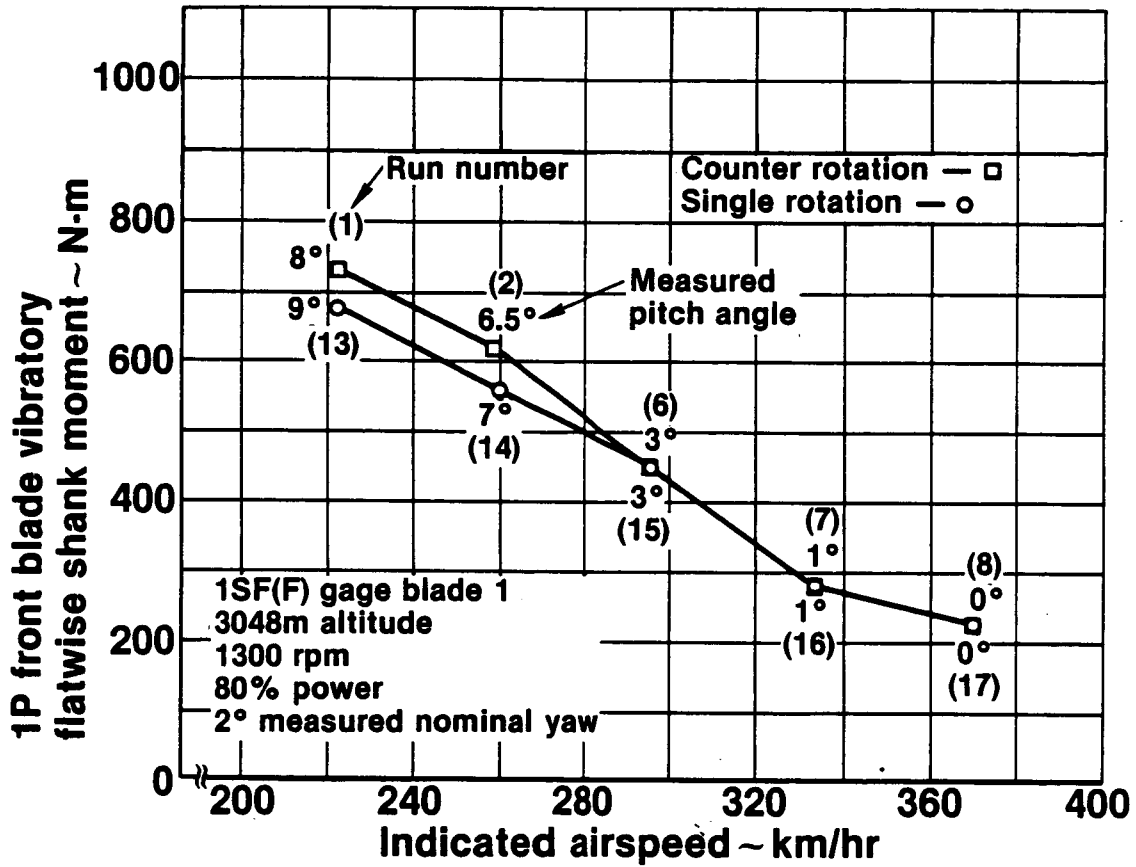


FIGURE 19. GANNET STABILIZED FLIGHT FRONT BLADE 1 FLATWISE 1P VIBRATORY SHANK MOMENT COMPARISON

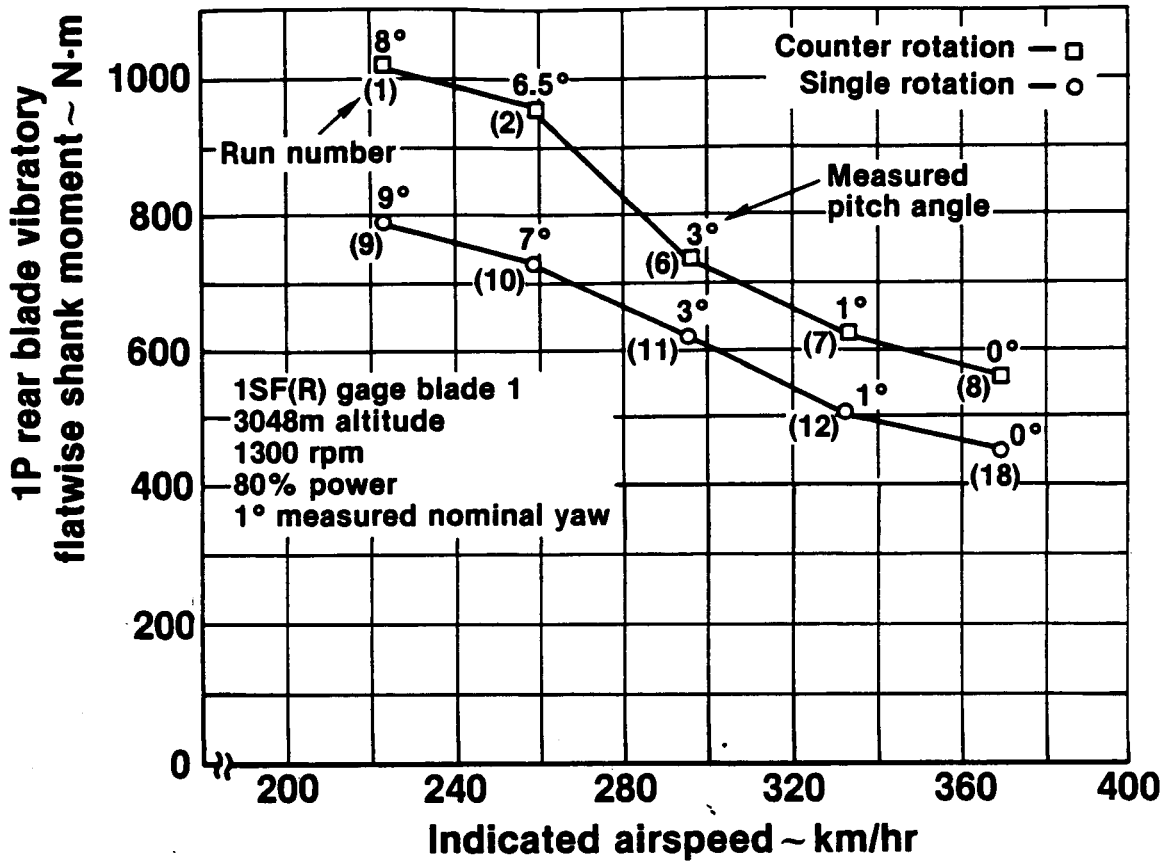


FIGURE 20. GANNET STABILIZED FLIGHT REAR BLADE 1 FLATWISE 1P VIBRATORY SHANK MOMENT COMPARISON

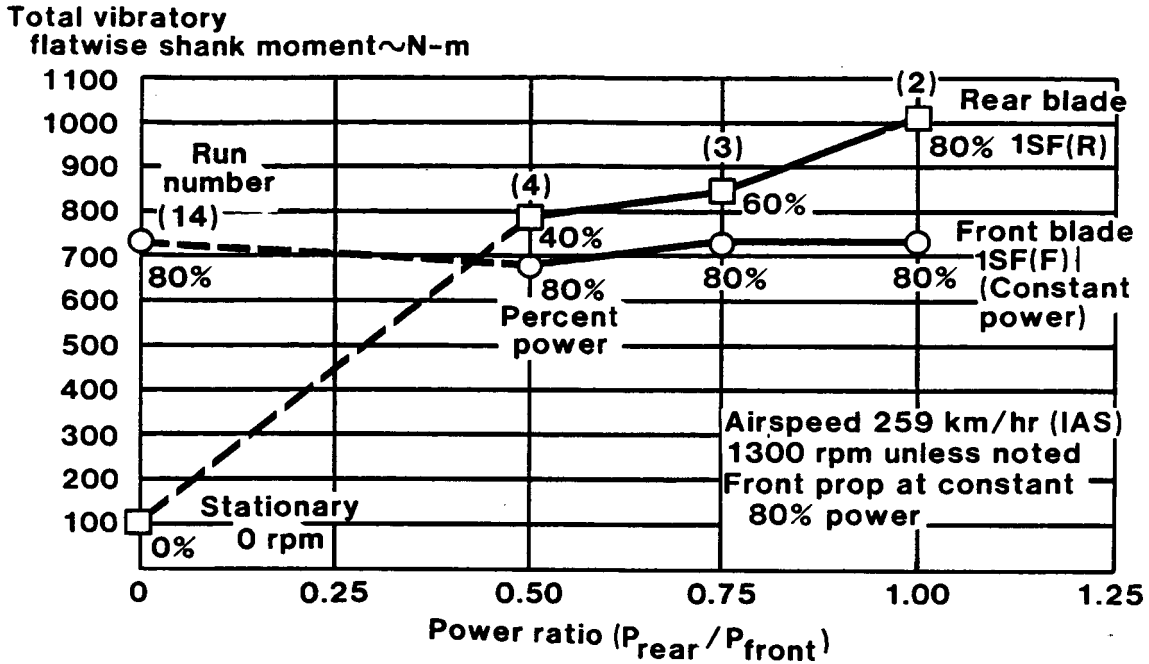


FIGURE 21. THE EFFECT OF REAR PROPELLER POWER ON THE FRONT BLADE RESPONSE FOR THE GANNET AIRCRAFT

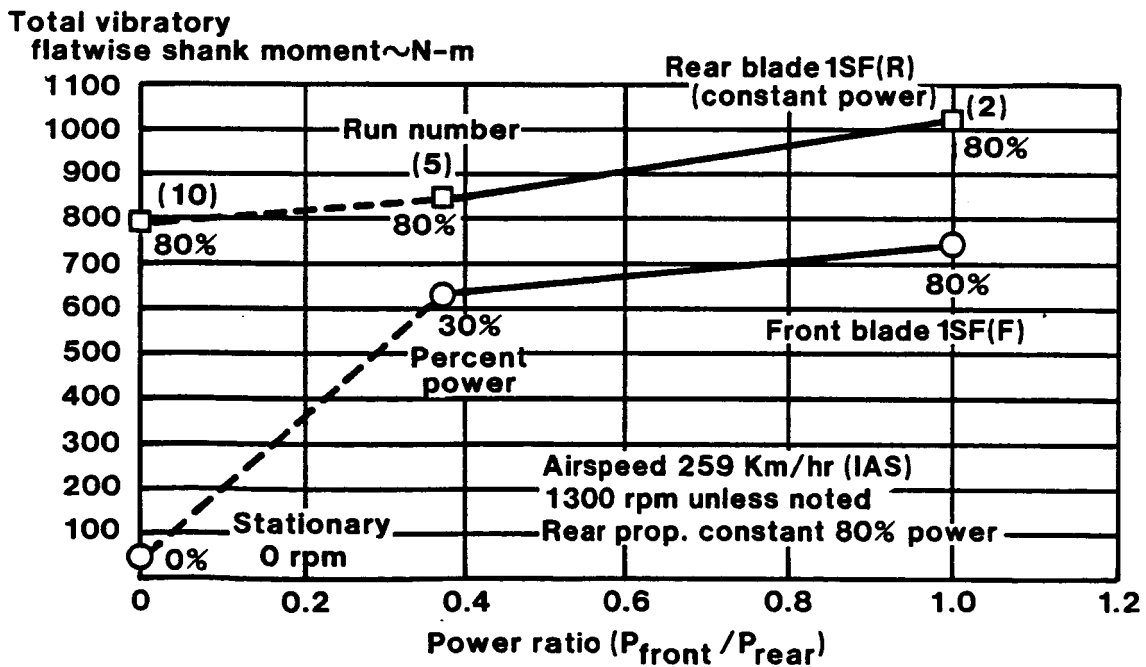


FIGURE 22. THE EFFECT OF FRONT BLADE POWER ON THE REAR BLADE RESPONSE FOR THE GANNET AIRCRAFT

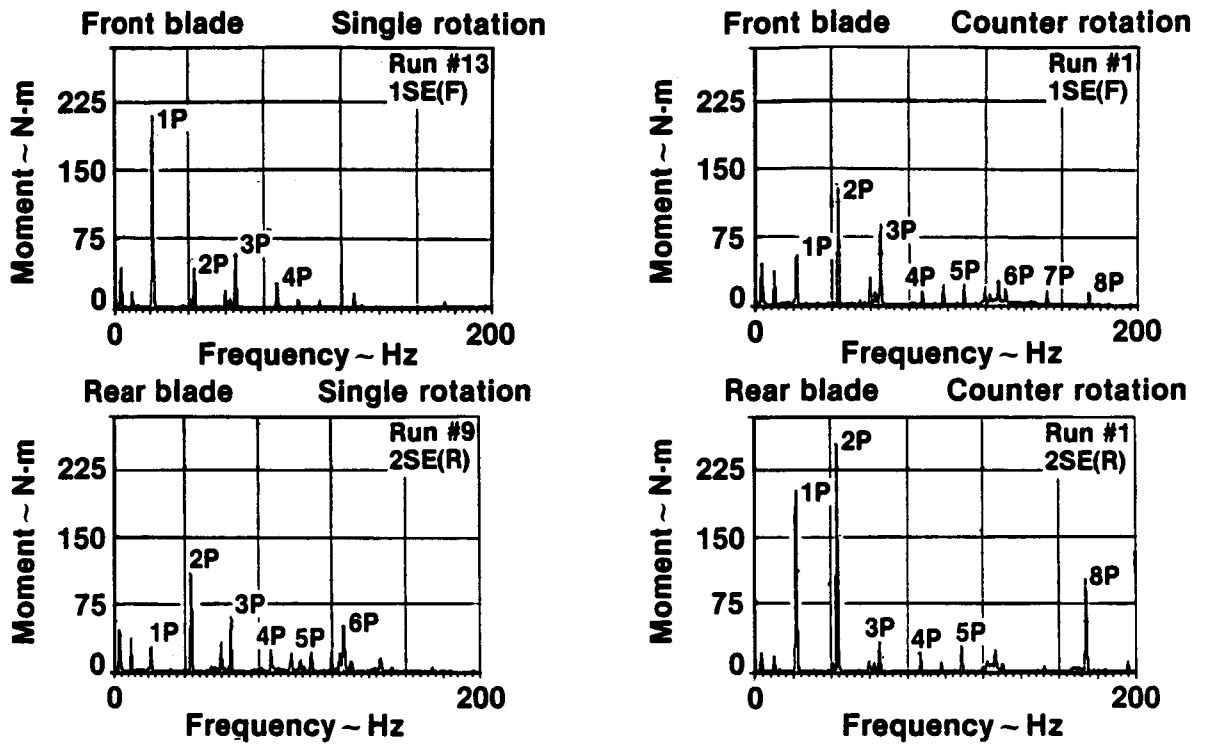


FIGURE 23. EDGEWISE SHANK BENDING MOMENT COMPONENTS FOR GANNET LOW SPEED FLIGHT 222 KM/HR

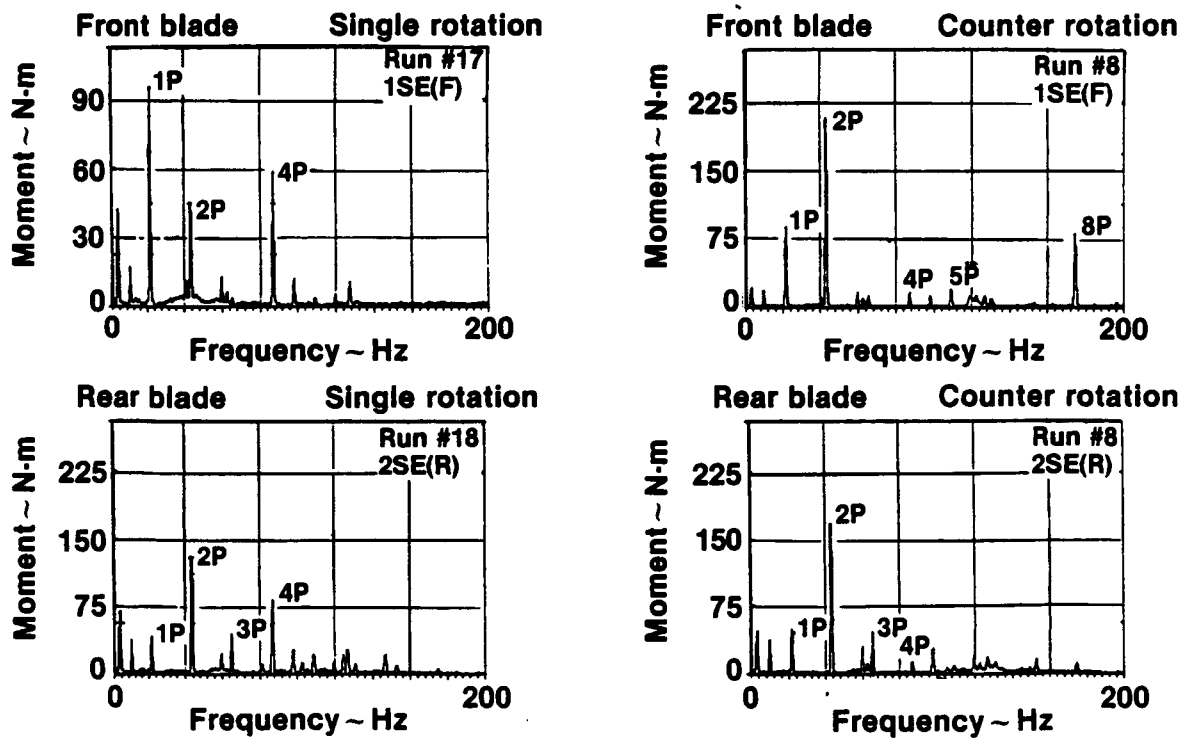


FIGURE 24. EDGEWISE SHANK BENDING MOMENT COMPONENTS FOR GANNET HIGH SPEED FLIGHT 370 KM/HR

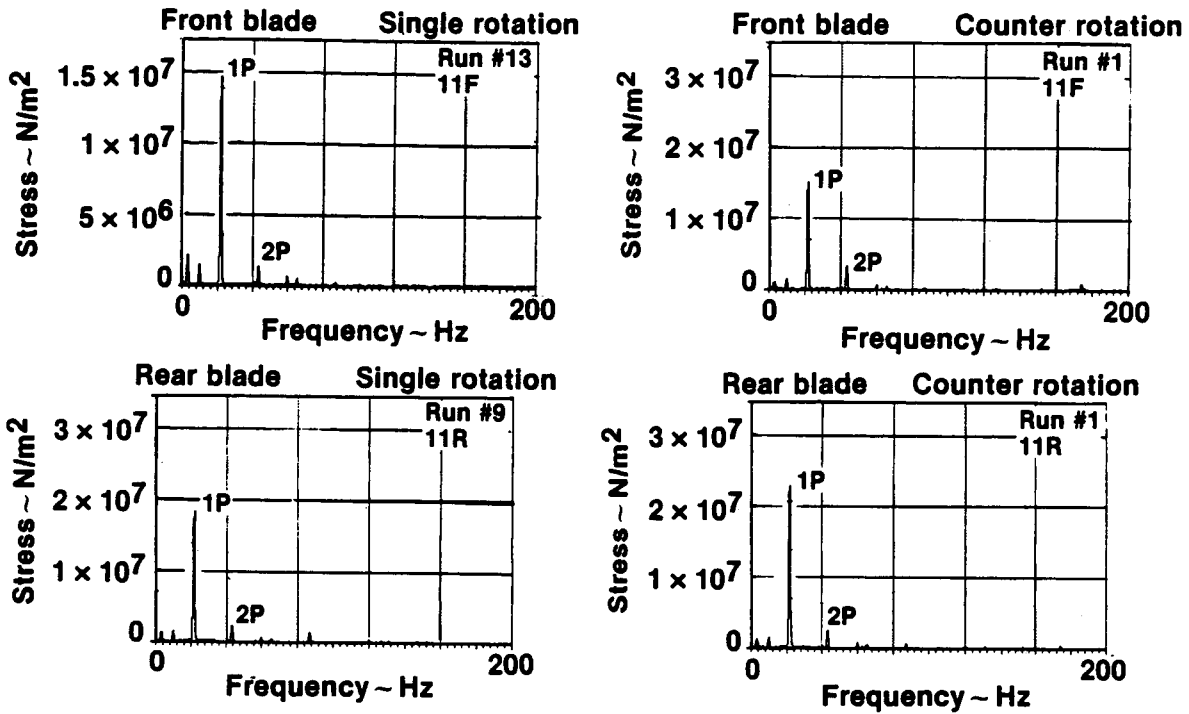


FIGURE 25. INBOARD BLADE BENDING GAGE STRESS COMPONENTS FOR GANNET LOW SPEED FLIGHT 222 KM/HR

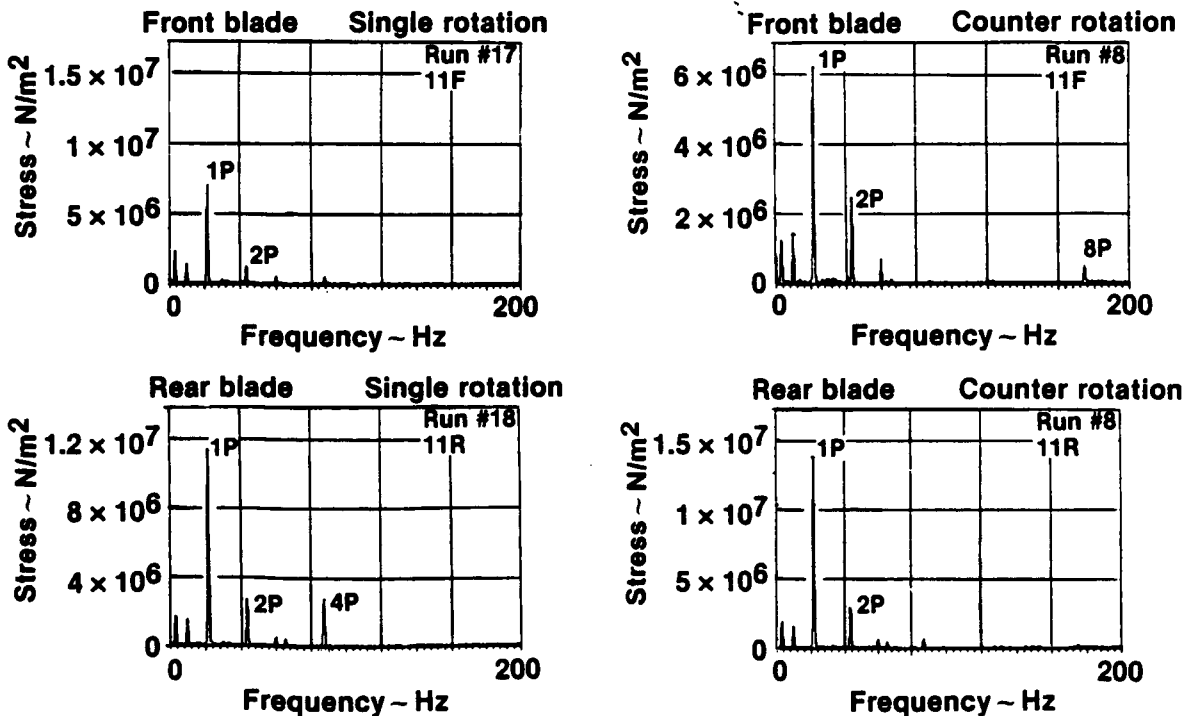


FIGURE 26. INBOARD BLADE BENDING GAGE STRESS COMPONENTS FOR GANNET HIGH SPEED FLIGHT 370 KM/HR

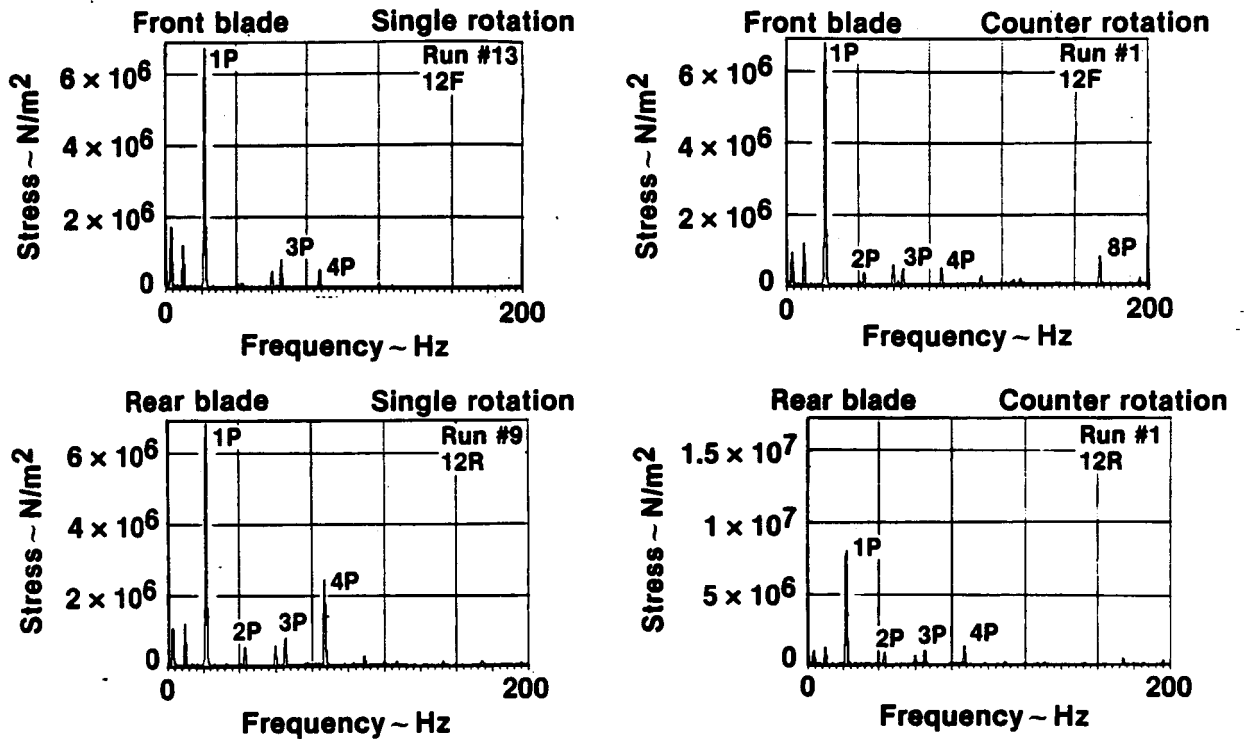


FIGURE 27. MID-BLADE BENDING GAGE STRESS COMPONENTS FOR GANNET LOW SPEED FLIGHT 222 KM/HR

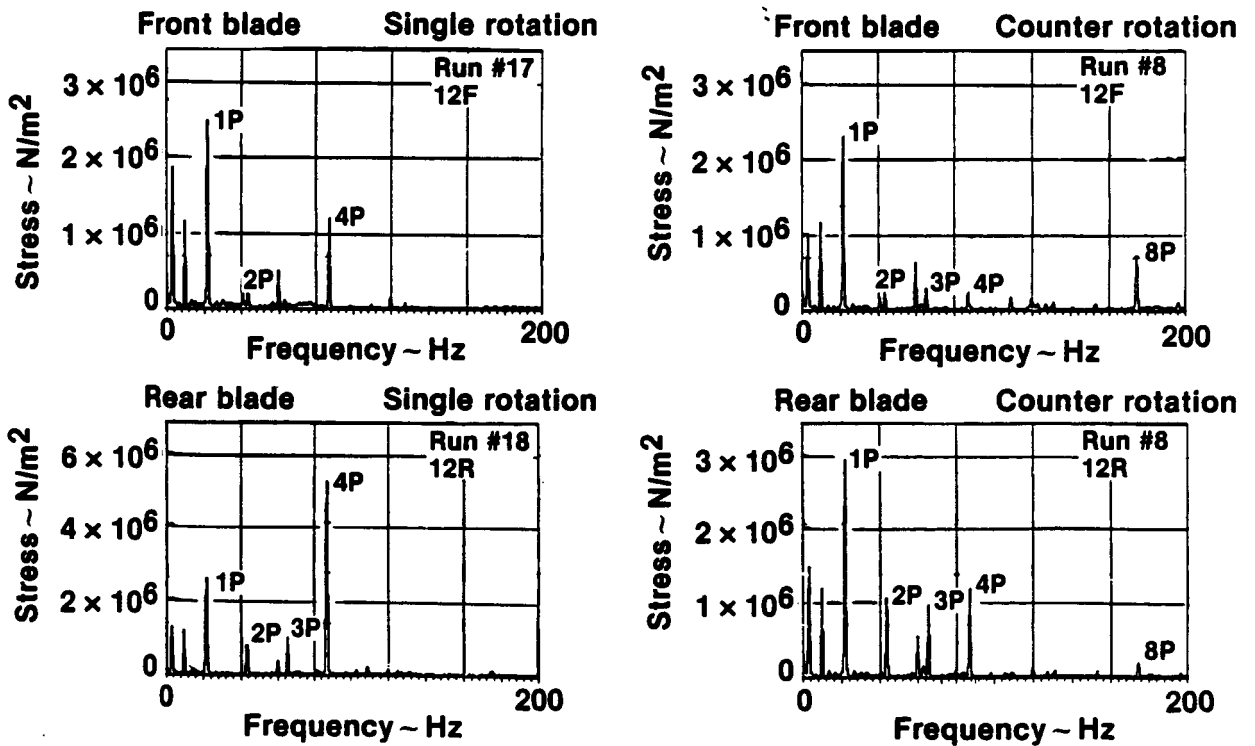


FIGURE 28. MID-BLADE BENDING GAGE STRESS COMPONENTS FOR GANNET HIGH SPEED FLIGHT 370 KM/HR

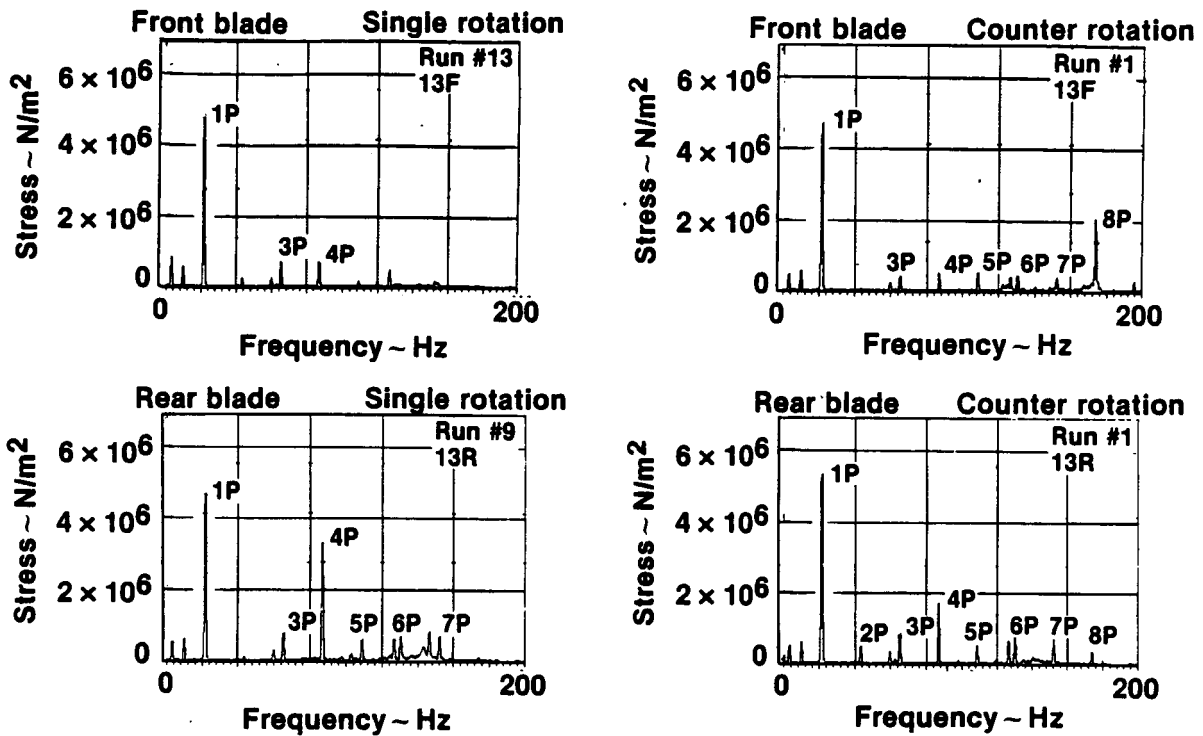


FIGURE 29. TIP BENDING GAGE STRESS COMPONENTS FOR GANNET LOW SPEED FLIGHT 222 KM/HR

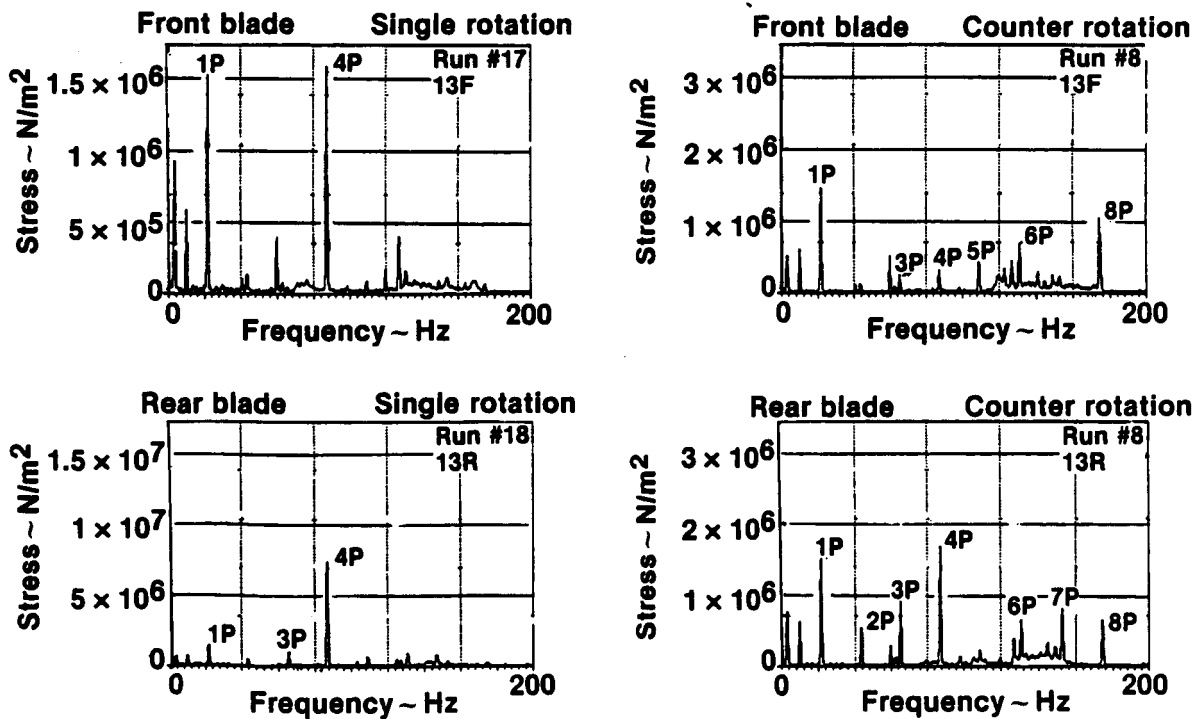


FIGURE 30. TIP BENDING GAGE STRESS COMPONENTS FOR GANNET HIGH SPEED FLIGHT 370 KM/HR

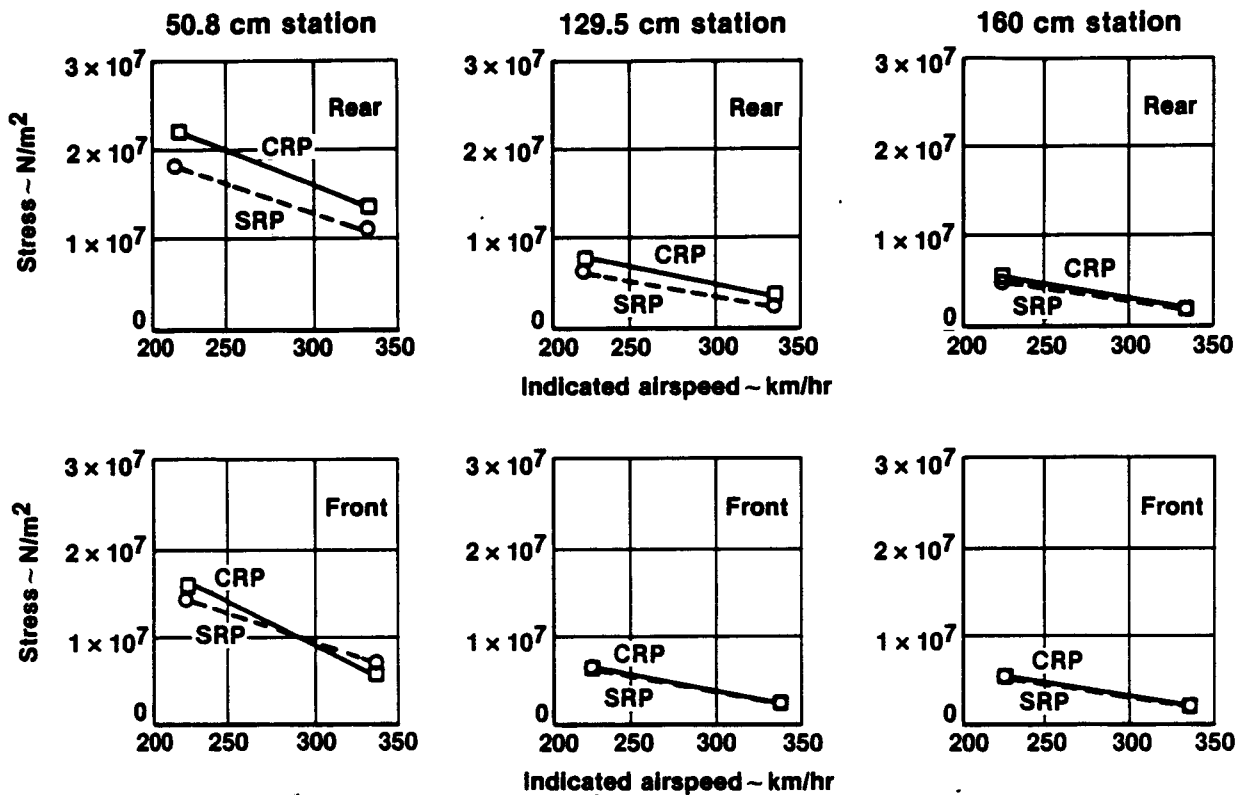


FIGURE 31. GANNET 1P BLADE VIBRATORY STRESS VARIATION WITH AIRSPEED

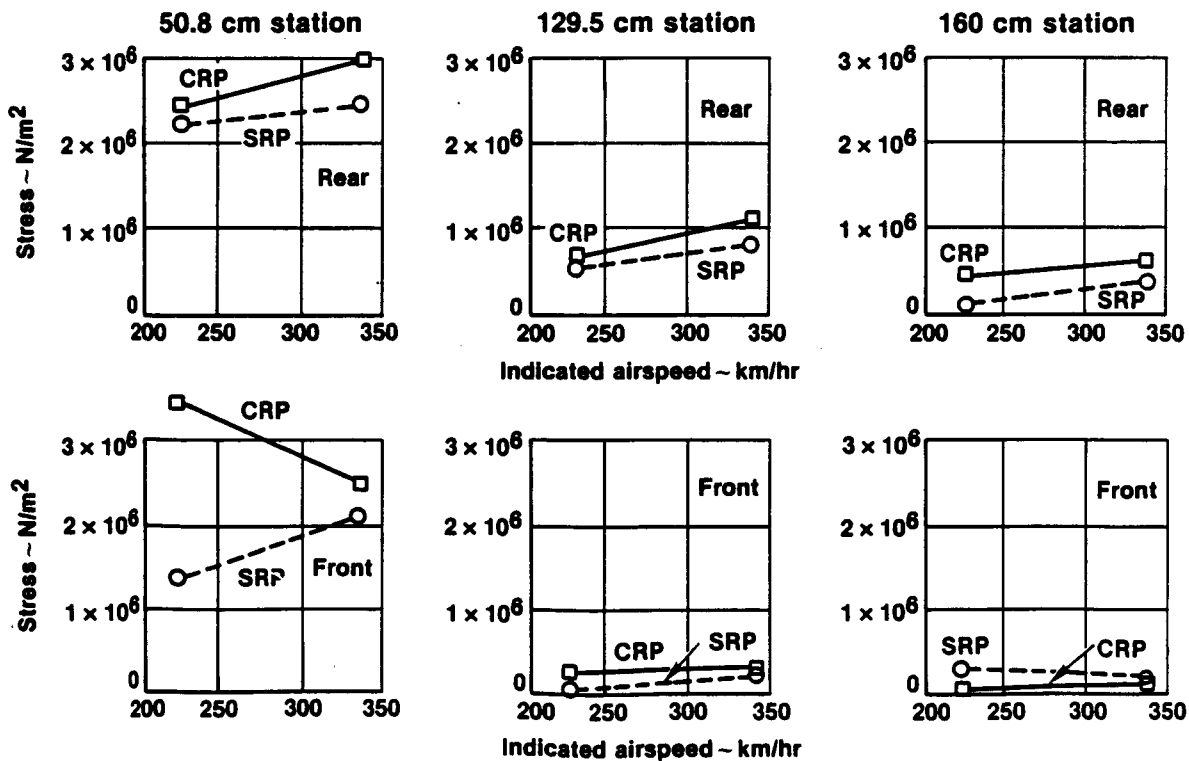


FIGURE 32. GANNET 2P BLADE VIBRATORY STRESS VARIATION WITH AIRSPEED

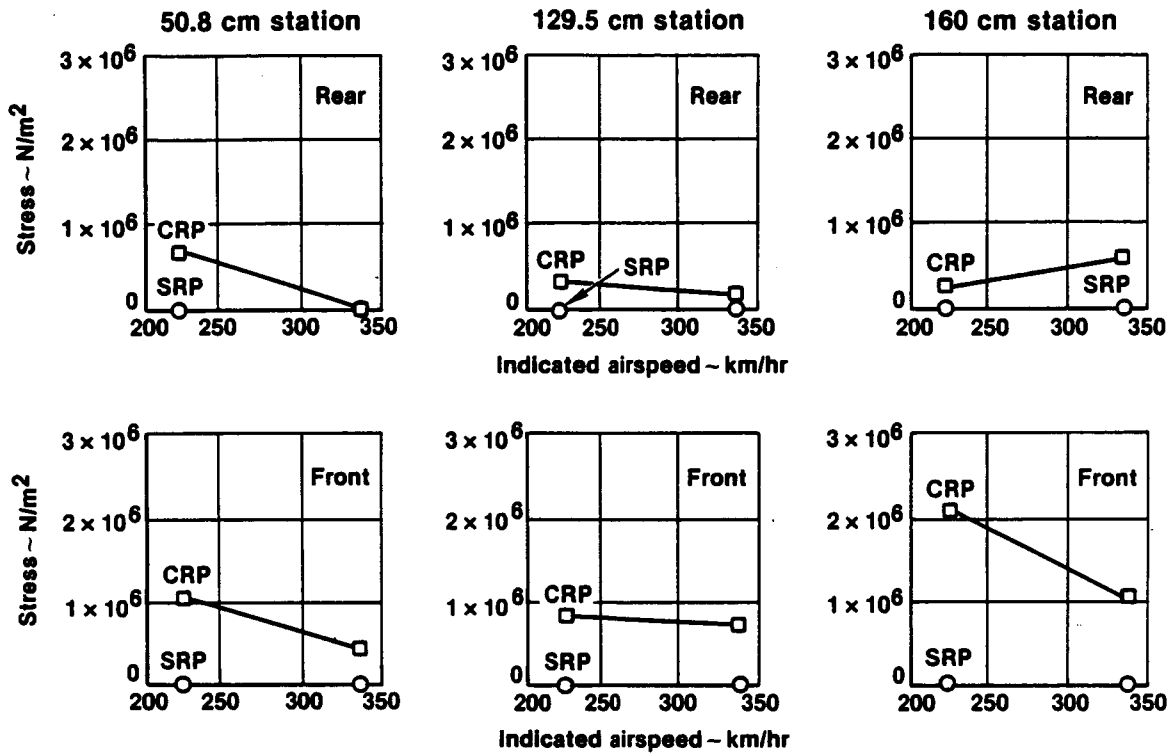


FIGURE 33. GANNET 8P BLADE VIBRATORY STRESS VARIATION WITH AIRSPEED

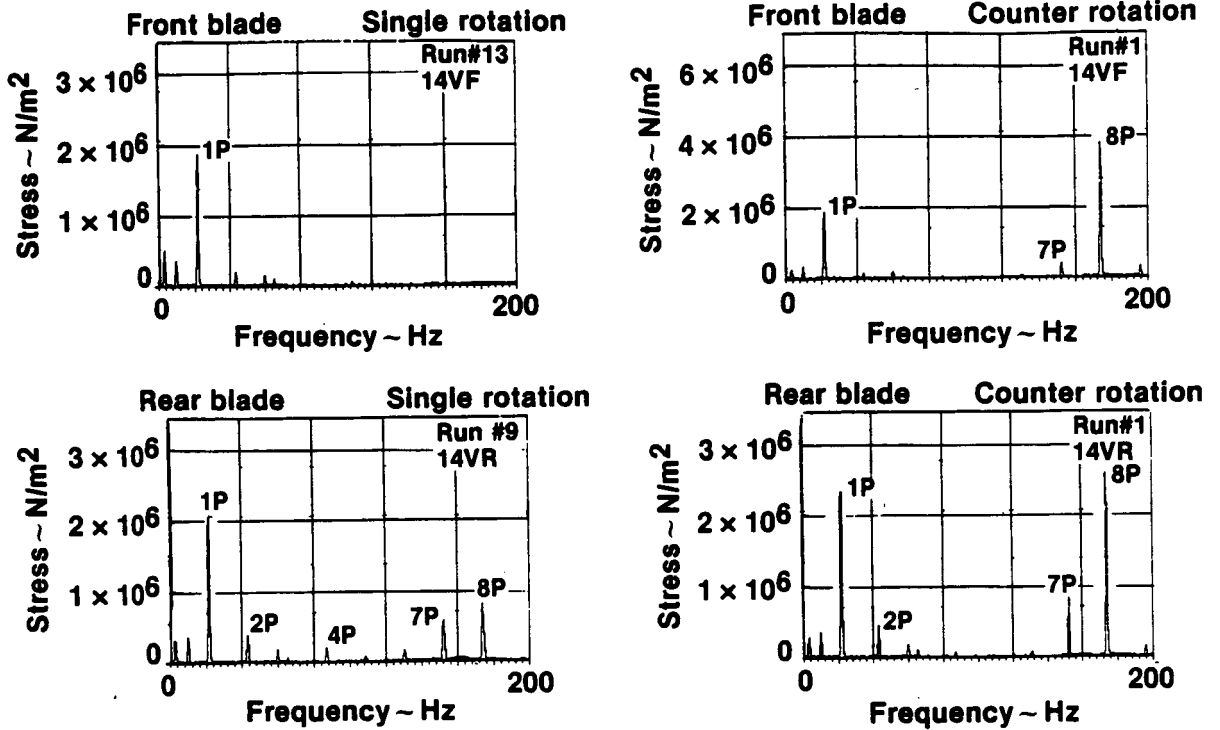


FIGURE 34. TORSIONAL RESPONSE COMPONENTS FOR GANNET LOW SPEED FLIGHT 222 KM/HR

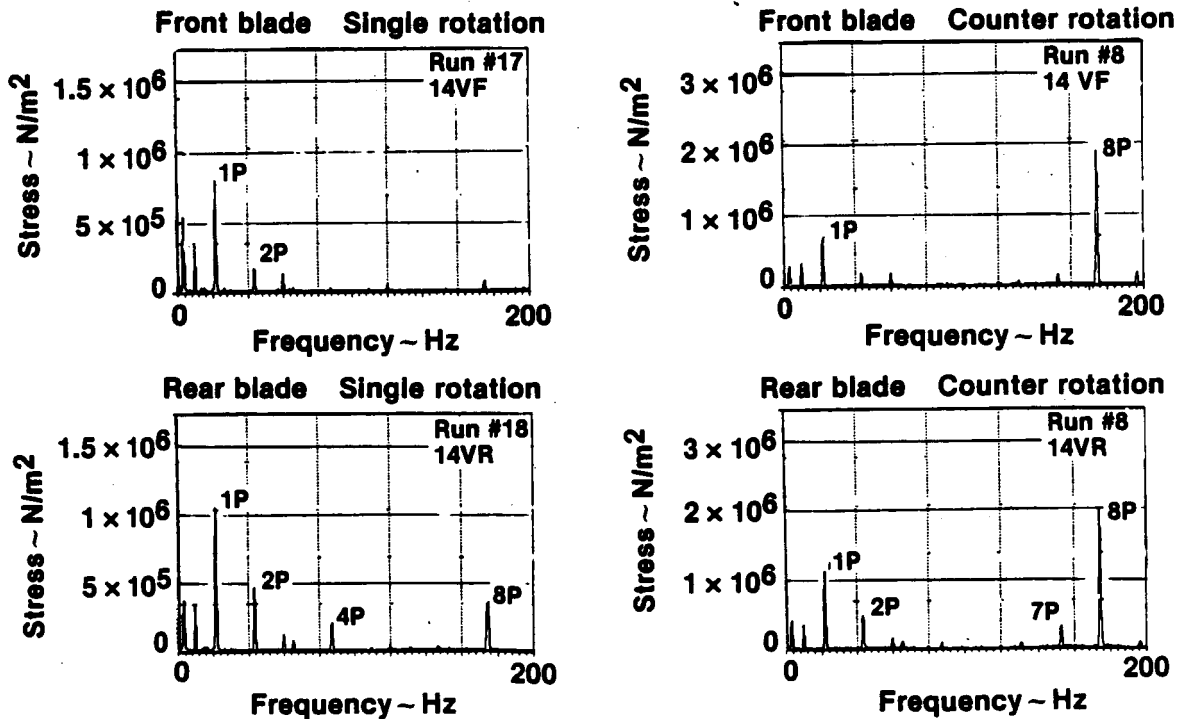


FIGURE 35. TORSIONAL RESPONSE COMPONENTS FOR GANNET HIGH SPEED FLIGHT 370 KM/HR

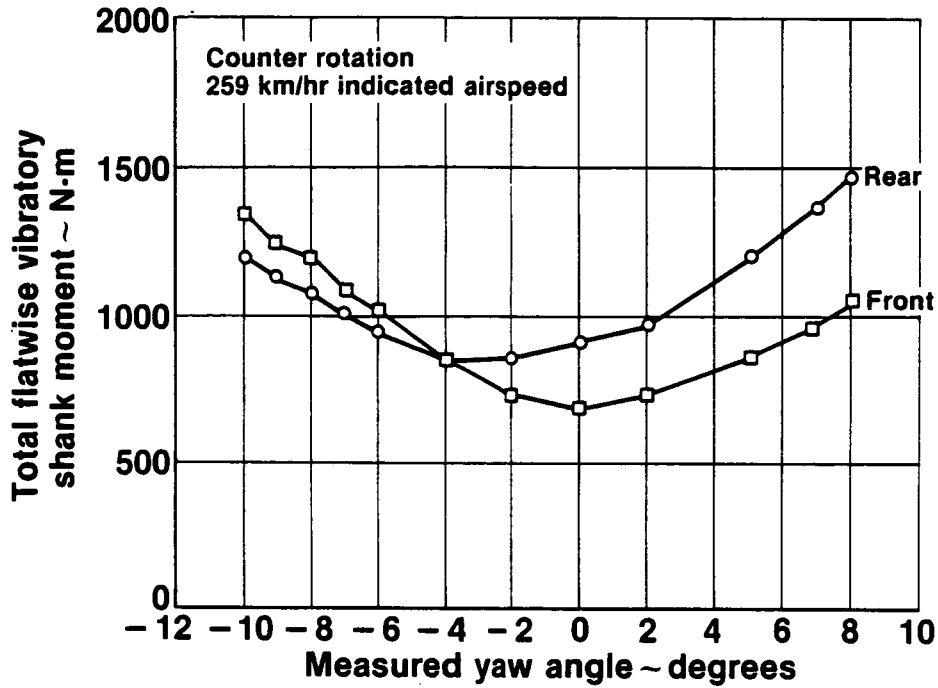


FIGURE 36. TOTAL FLATWISE VIBRATORY SHANK MOMENT FOR A LOW SPEED YAW MANEUVER ON THE GANNET AIRCRAFT

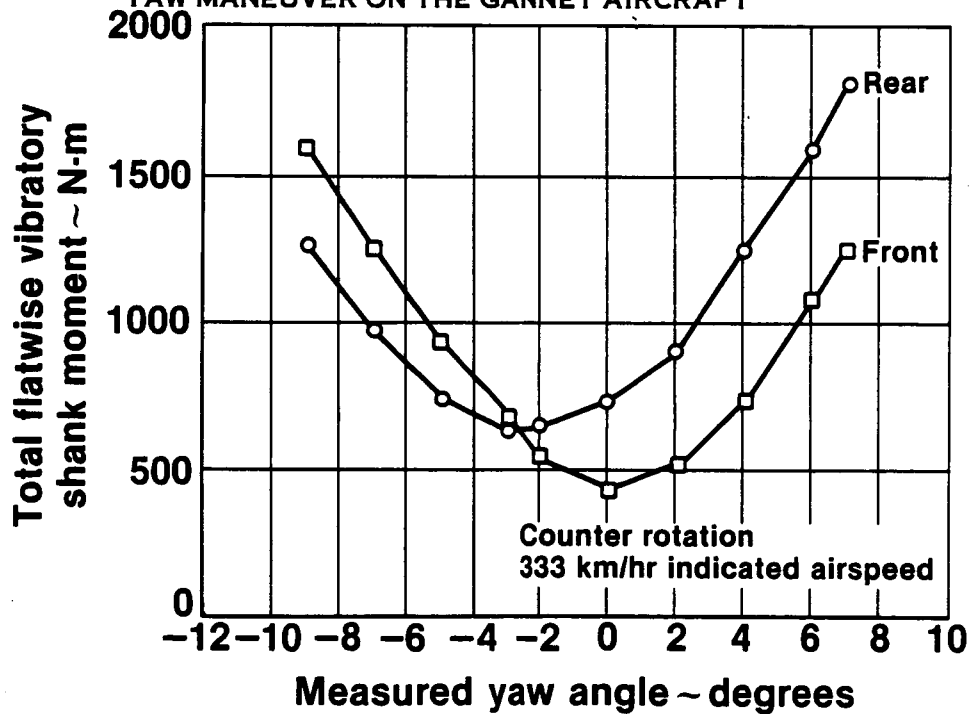


FIGURE 37. TOTAL FLATWISE VIBRATORY SHANK MOMENT FOR A HIGH SPEED YAW MANEUVER ON THE GANNET AIRCRAFT

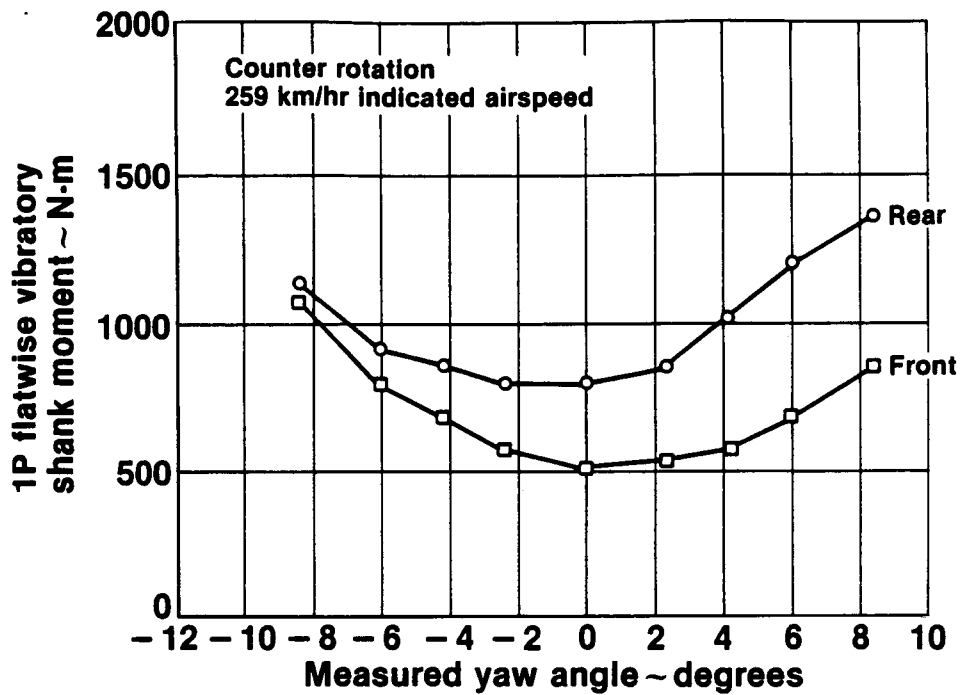


FIGURE 38. 1P FLATWISE VIBRATORY SHANK MOMENT FOR A LOW SPEED YAW MANEUVER ON THE GANNET AIRCRAFT

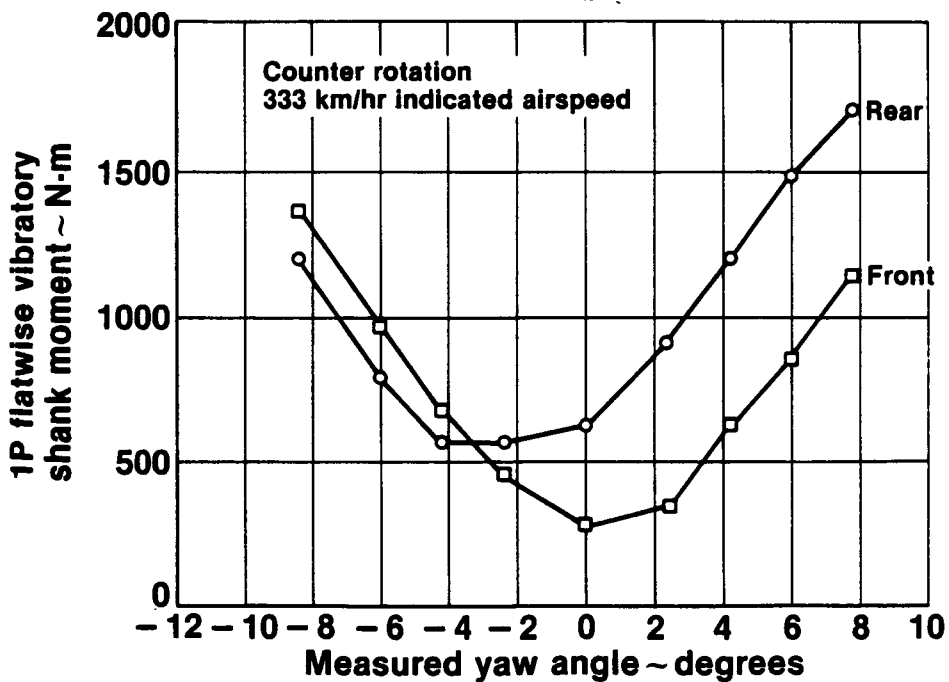


FIGURE 39. 1P FLATWISE VIBRATORY SHANK MOMENT FOR A HIGH SPEED YAW MANEUVER ON THE GANNET AIRCRAFT

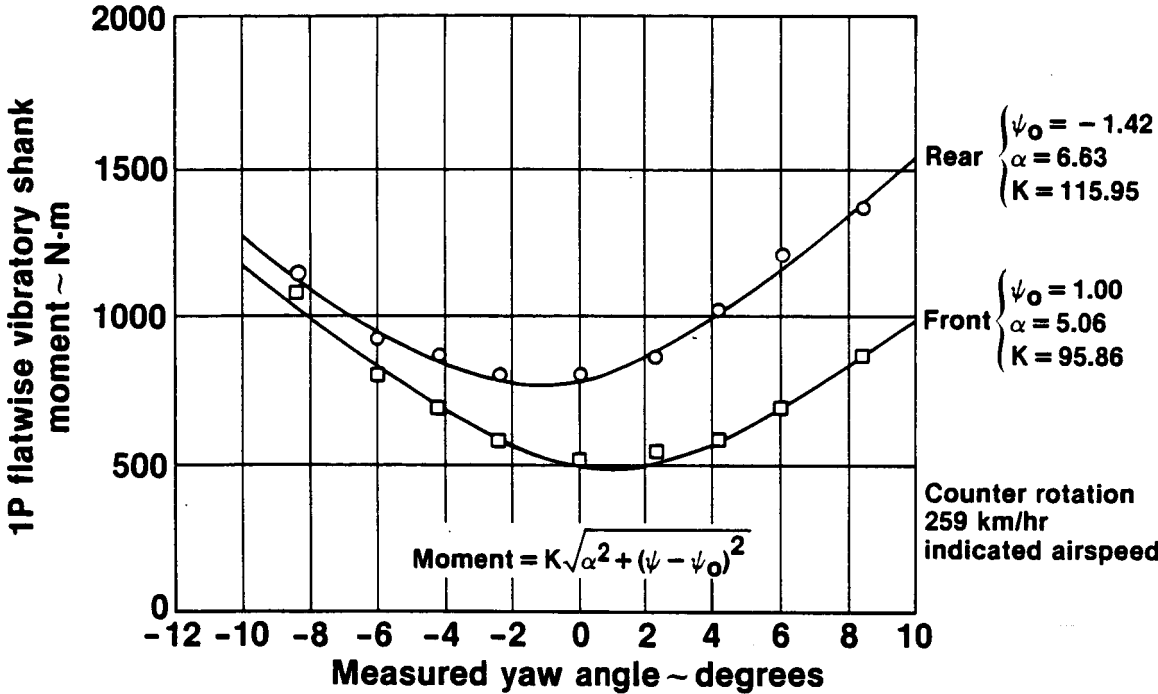


FIGURE 40. HYPERBOLIC CURVE FIT TO THE 1P FLATWISE VIBRATORY SHANK MOMENT FOR A LOW SPEED YAW MANEUVER ON THE GANNET AIRCRAFT

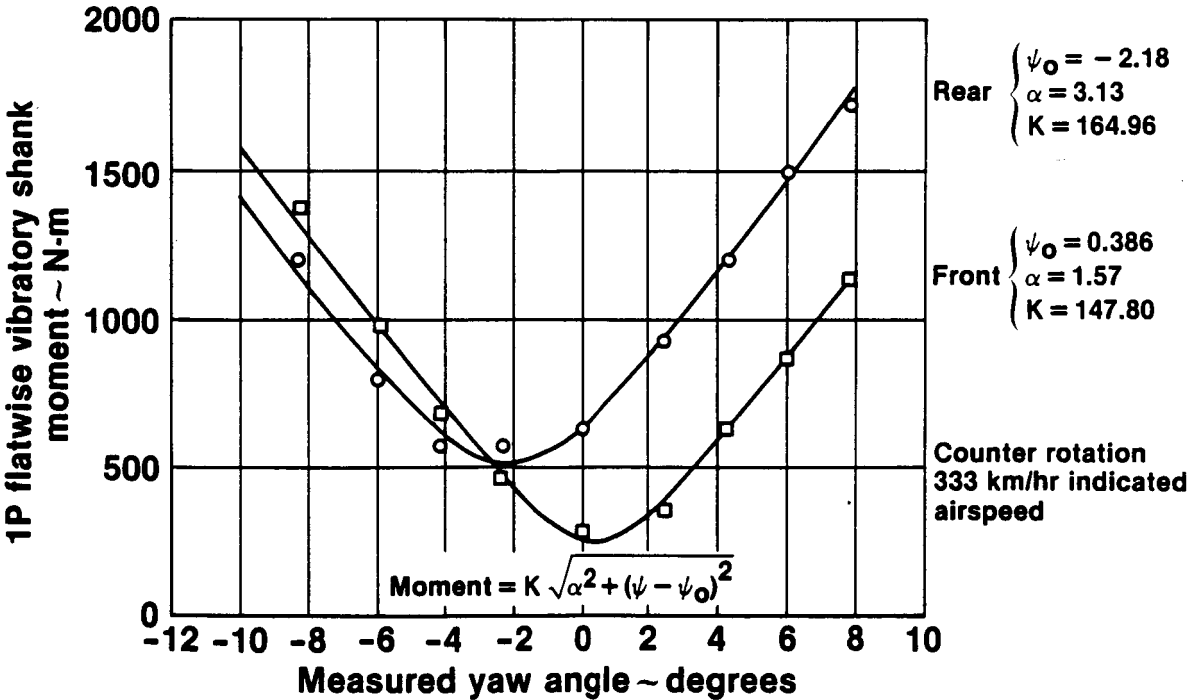


FIGURE 41. HYPERBOLIC CURVE FIT TO THE 1P FLATWISE VIBRATORY SHANK MOMENT FOR A HIGH SPEED YAW MANEUVER ON THE GANNET AIRCRAFT

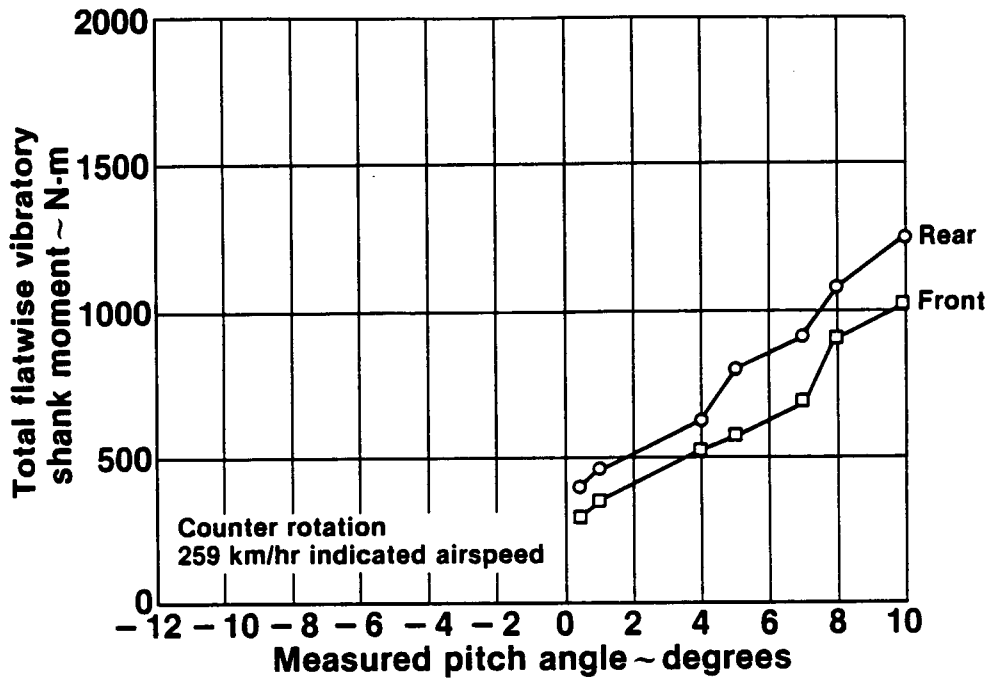


FIGURE 42. TOTAL FLATWISE VIBRATORY SHANK MOMENT FOR A LOW SPEED PITCH MANEUVER ON THE GANNET AIRCRAFT

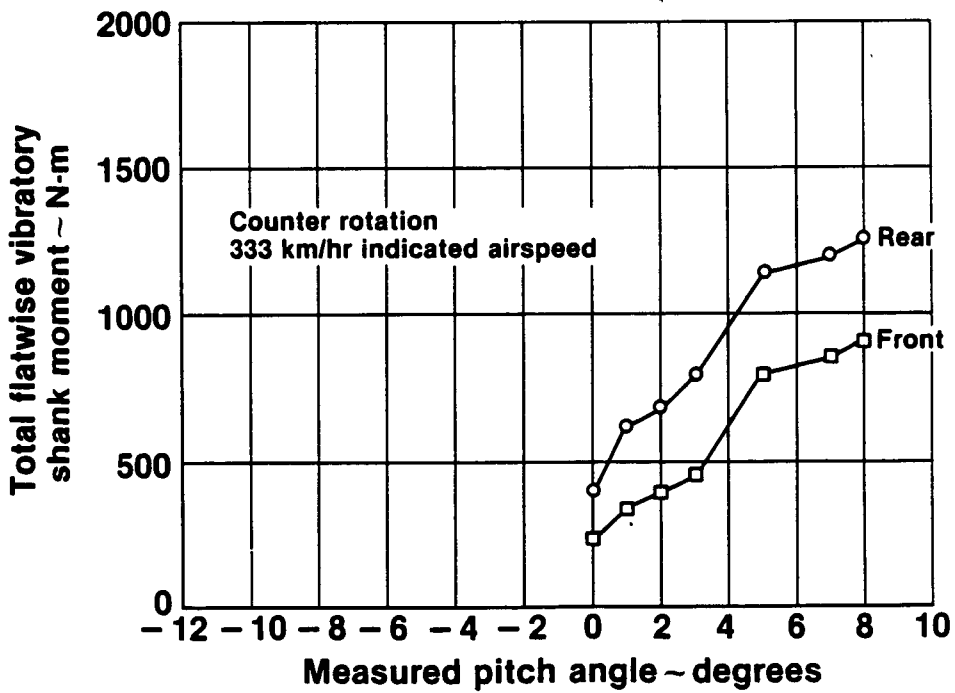


FIGURE 43. TOTAL FLATWISE VIBRATORY SHANK MOMENT FOR A HIGH SPEED PITCH MANEUVER ON THE GANNET AIRCRAFT

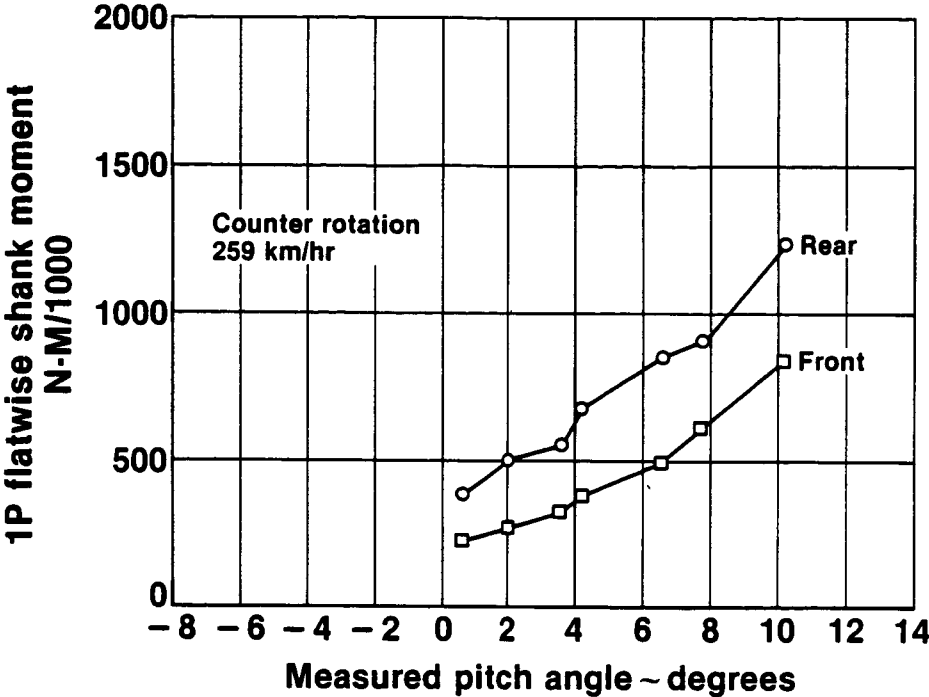


FIGURE 44. 1P FLATWISE VIBRATORY SHANK MOMENT FOR A LOW SPEED PITCH MANEUVER ON THE GANNET AIRCRAFT

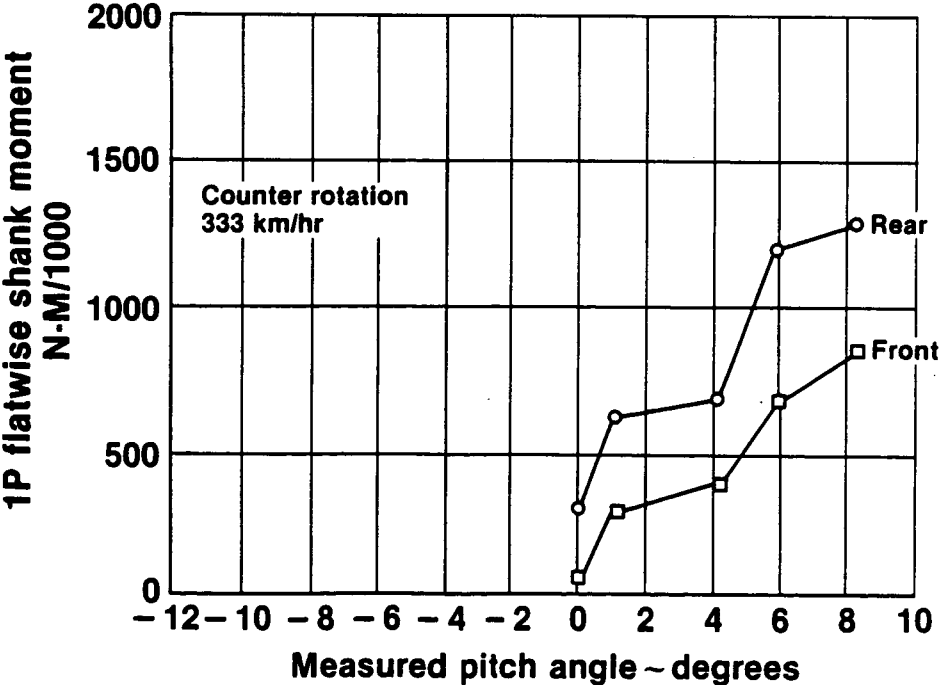


FIGURE 45. 1P FLATWISE VIBRATORY SHANK MOMENT FOR A HIGH SPEED PITCH MANEUVER ON THE GANNET AIRCRAFT

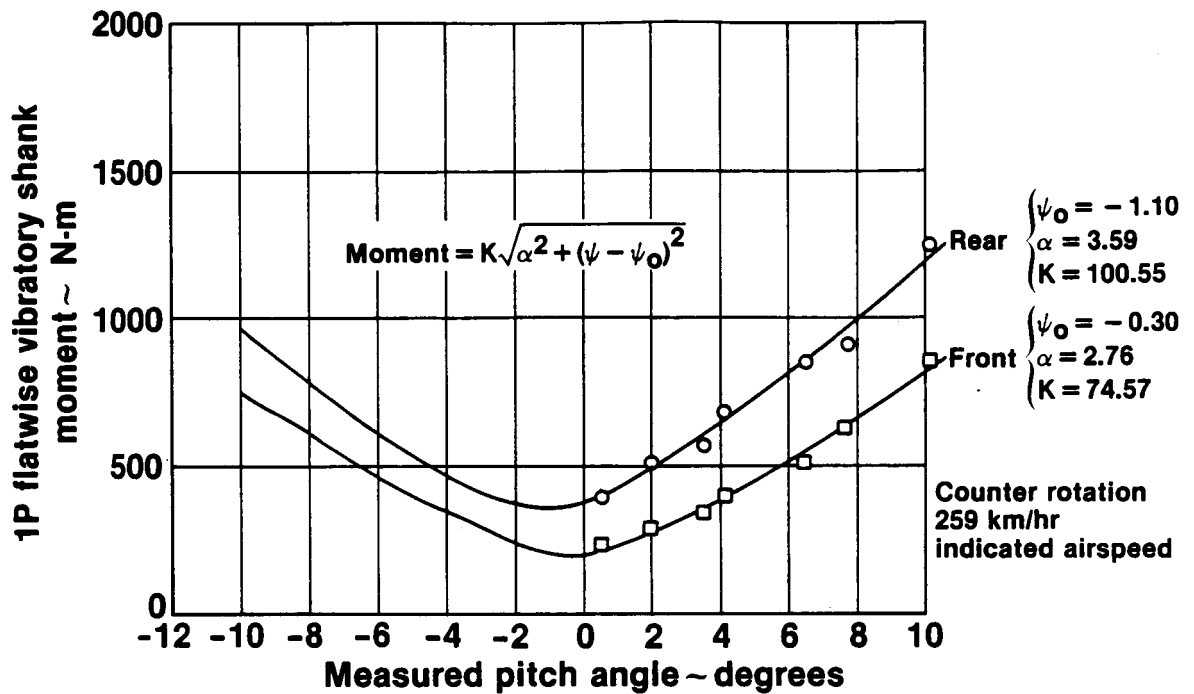


FIGURE 46. HYPERBOLIC CURVE FIT TO THE 1P FLATWISE VIBRATORY SHANK MOMENT FOR A LOW SPEED PITCH MANEUVER ON THE GANNET AIRCRAFT

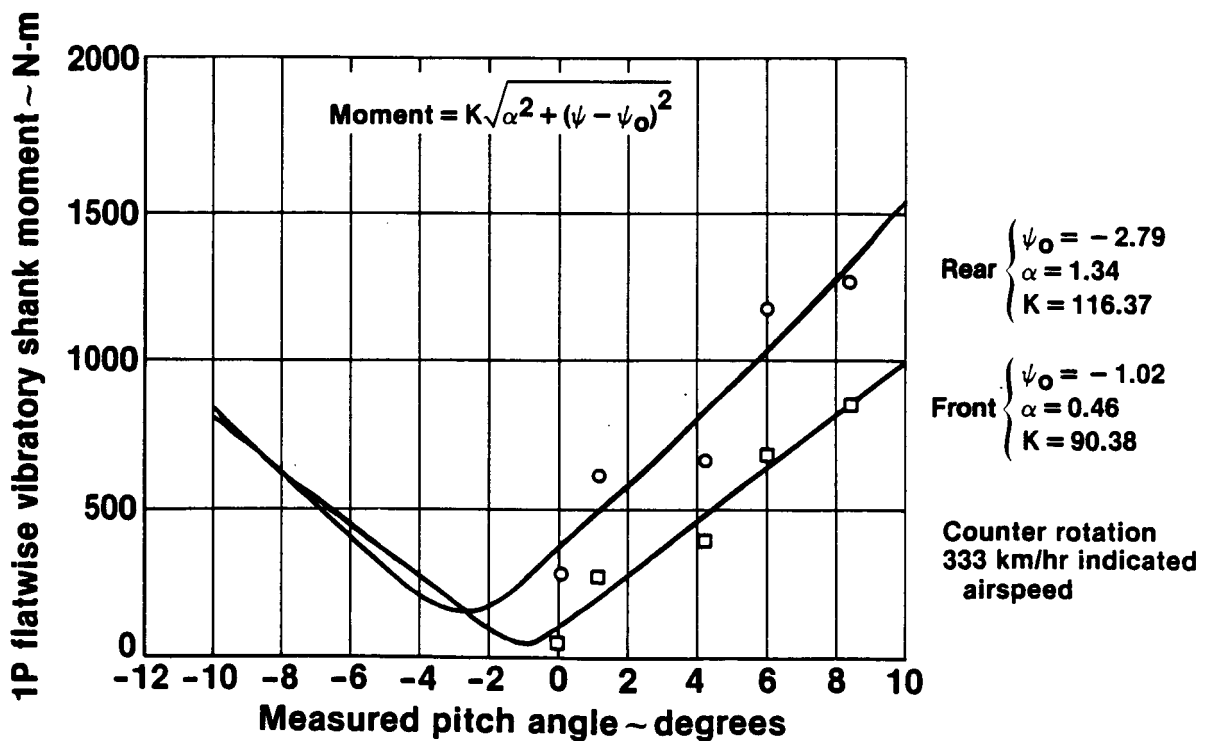


FIGURE 47. HYPERBOLIC CURVE FIT TO THE 1P FLATWISE VIBRATORY SHANK MOMENT FOR A HIGH SPEED PITCH MANEUVER ON THE GANNET AIRCRAFT

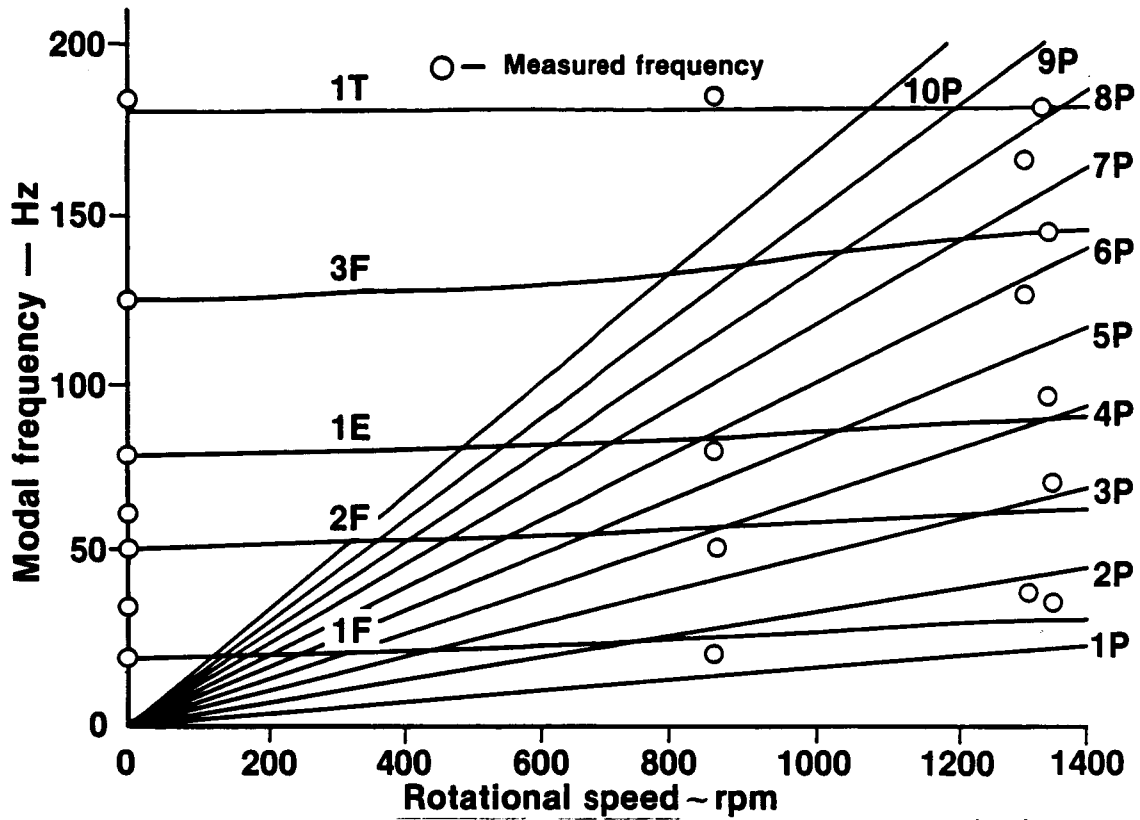


FIGURE 48. CALCULATED AND MEASURED GANNET FRONT BLADE MODAL FREQUENCIES

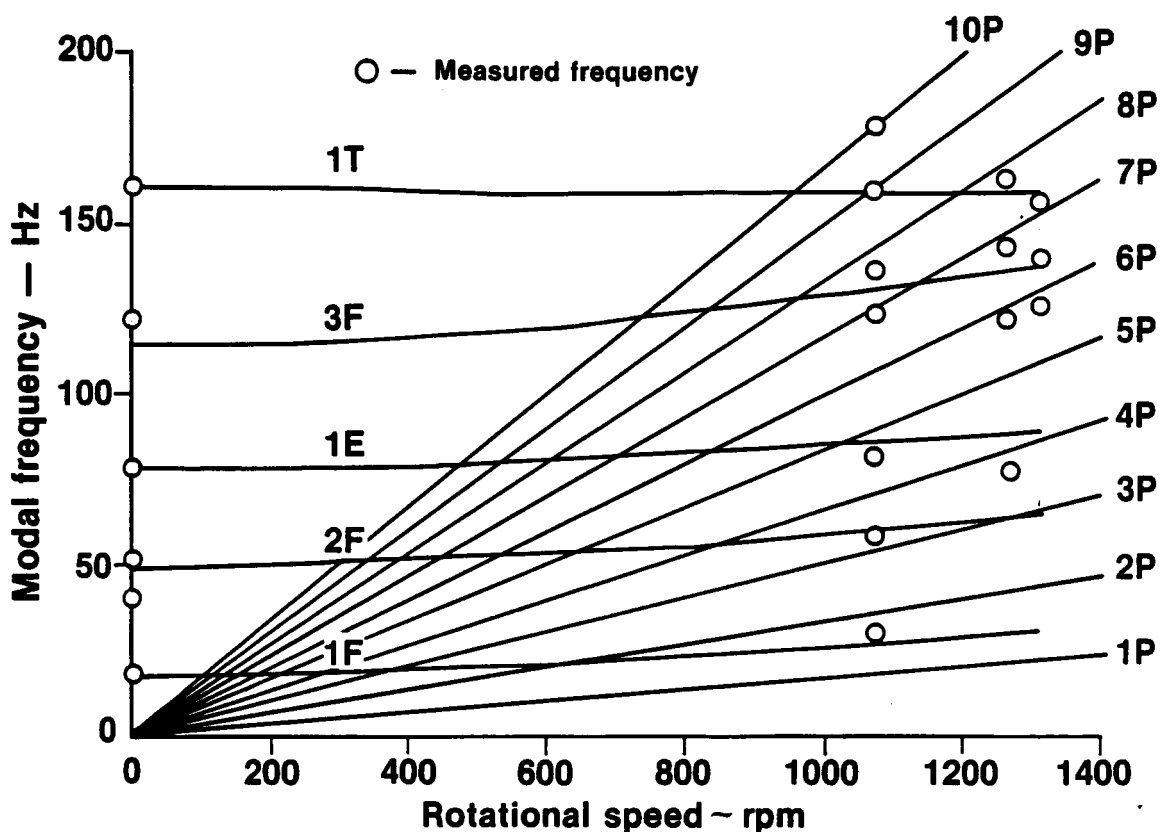


FIGURE 49. CALCULATED AND MEASURED GANNET REAR BLADE MODAL FREQUENCIES

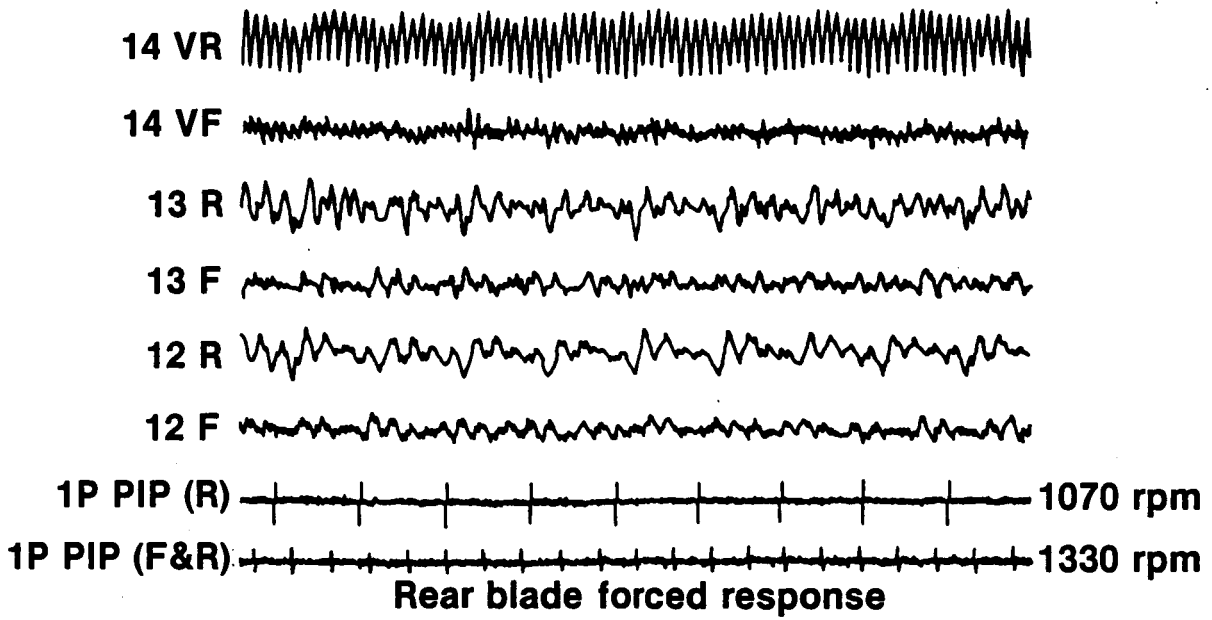


FIGURE 50. SAMPLE GANNET GROUND RESPONSE DATA SHOWING THE FIRST TORSION MODE CRITICAL SPEED AT $(RPM[F]+RPM[R]) \times 4 = 160$ HZ ON THE 14VR STRAIN GAGE

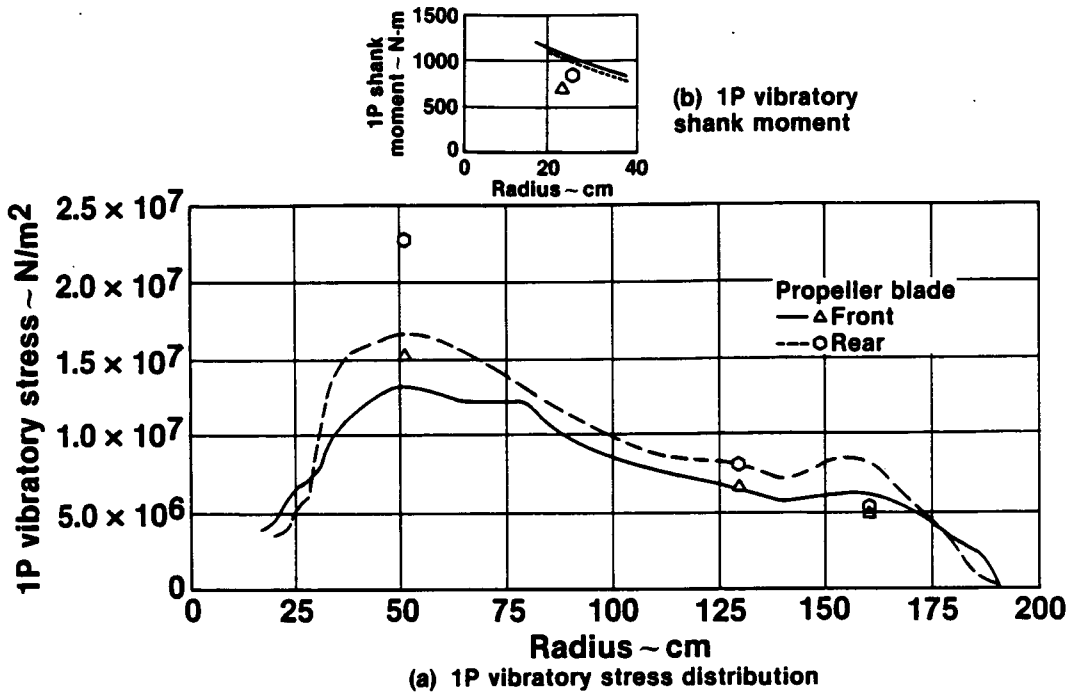


FIGURE 51. COMPARISON OF GANNET COUNTER ROTATION 1P TEST DATA TO THEORETICAL RESULTS FOR LOW SPEED STABILIZED FLIGHT 222 KM/HR

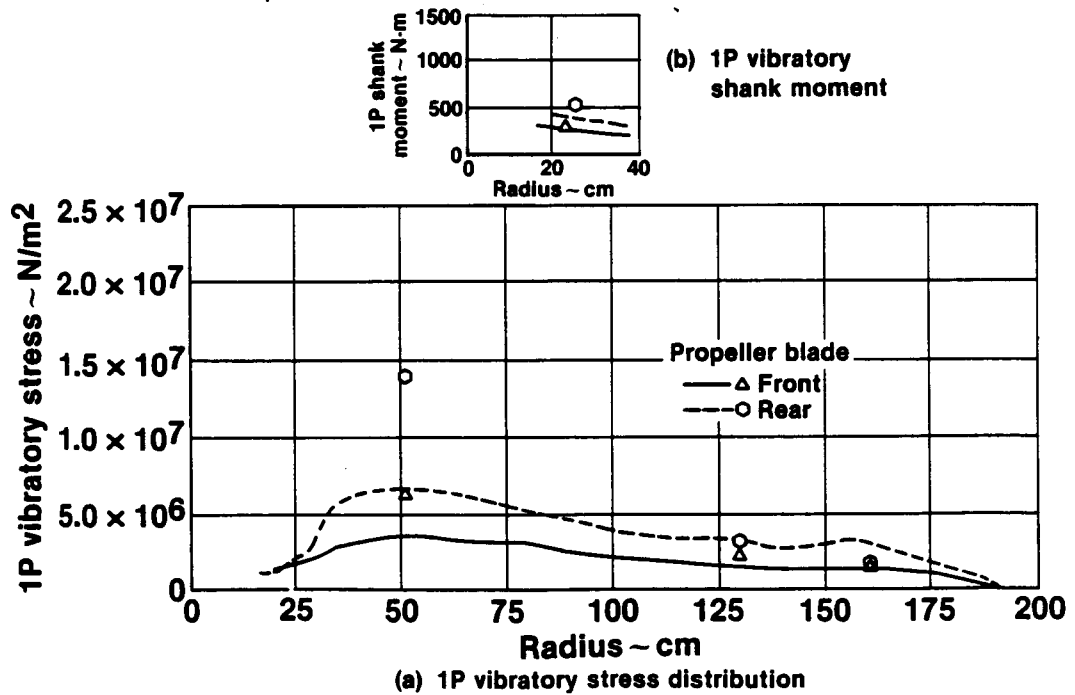


FIGURE 52. COMPARISON OF GANNET COUNTER ROTATION 1P TEST DATA TO THEORETICAL RESULTS FOR HIGH SPEED STABILIZED FLIGHT 370 KM/HR

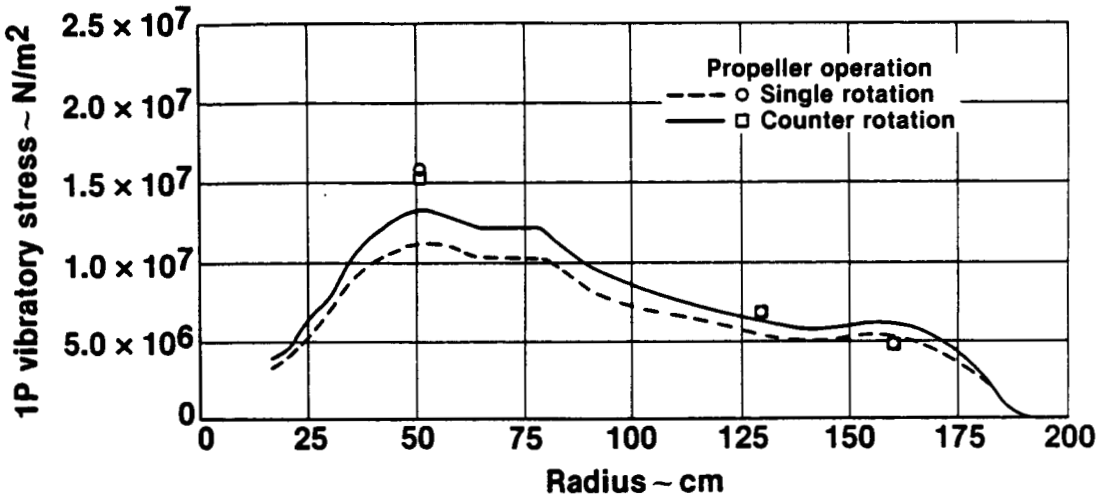


FIGURE 53. COMPARISON OF GANNET FRONT BLADE 1P TEST DATA TO THEORETICAL STRESS DISTRIBUTIONS FOR BOTH SINGLE AND COUNTER ROTATION OPERATION DURING LOW SPEED FLIGHT 222 KM/HR

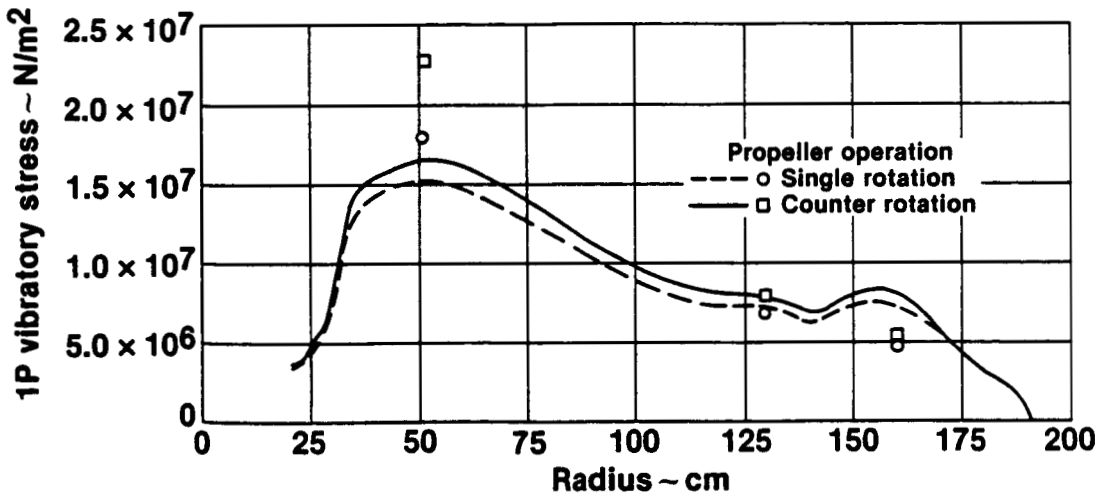


FIGURE 54. COMPARISON OF GANNET REAR BLADE 1P TEST DATA TO THEORETICAL STRESS DISTRIBUTIONS FOR BOTH SINGLE AND COUNTER ROTATION OPERATION DURING LOW SPEED FLIGHT 222 KM/HR

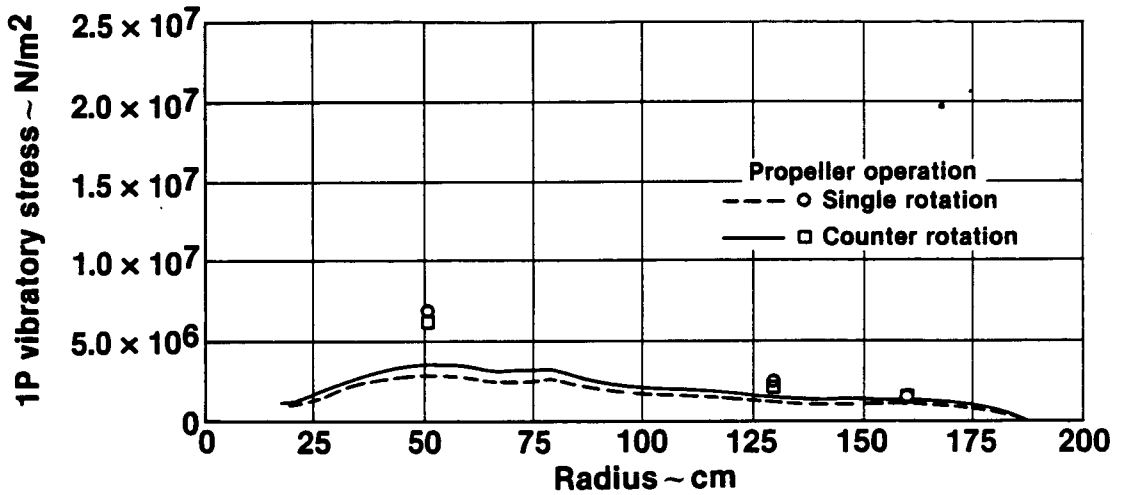


FIGURE 55. COMPARISON OF GANNET FRONT BLADE 1P TEST DATA TO THEORETICAL STRESS DISTRIBUTIONS FOR BOTH SINGLE AND COUNTER ROTATION OPERATION DURING HIGH SPEED FLIGHT 370 KM/HR

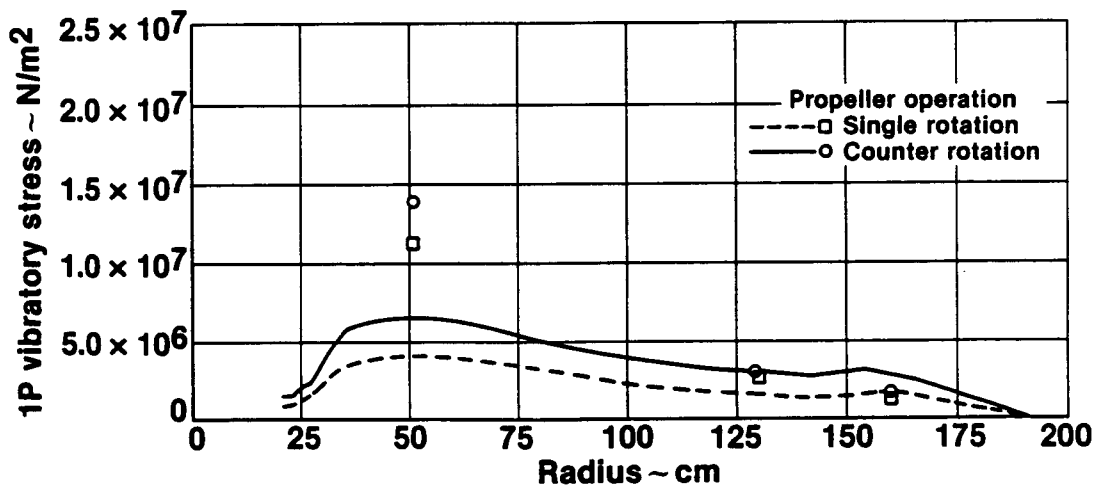


FIGURE 56. COMPARISON OF GANNET REAR BLADE 1P TEST DATA TO THEORETICAL STRESS DISTRIBUTIONS FOR BOTH SINGLE AND COUNTER ROTATION OPERATION DURING HIGH SPEED FLIGHT 370 KM/HR

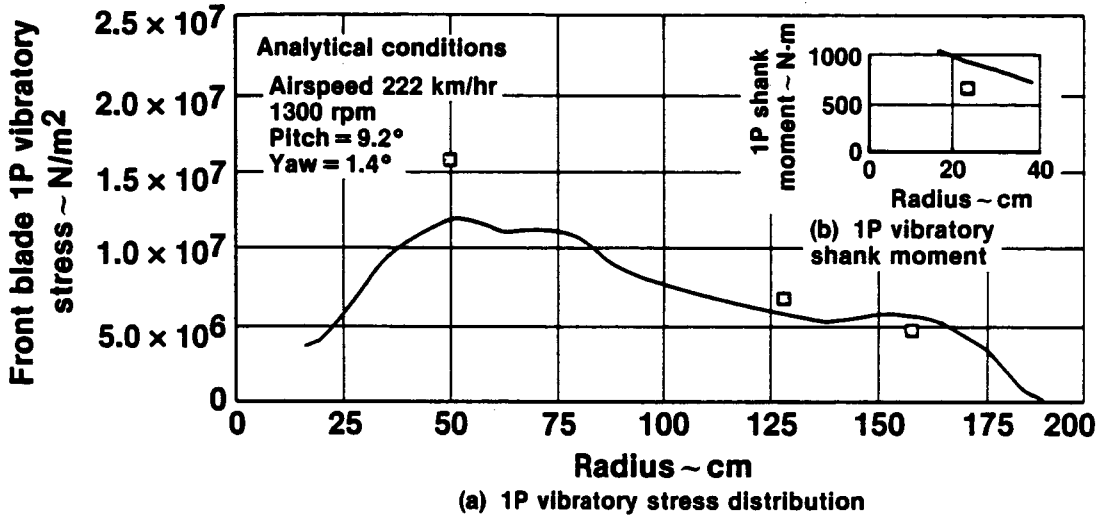


FIGURE 57. COMPARISON OF GANNET FRONT BLADE SINGLE ROTATION 1P TEST DATA TO THEORETICAL RESULTS FOR LOW SPEED STABILIZED FLIGHT 222 KM/HR

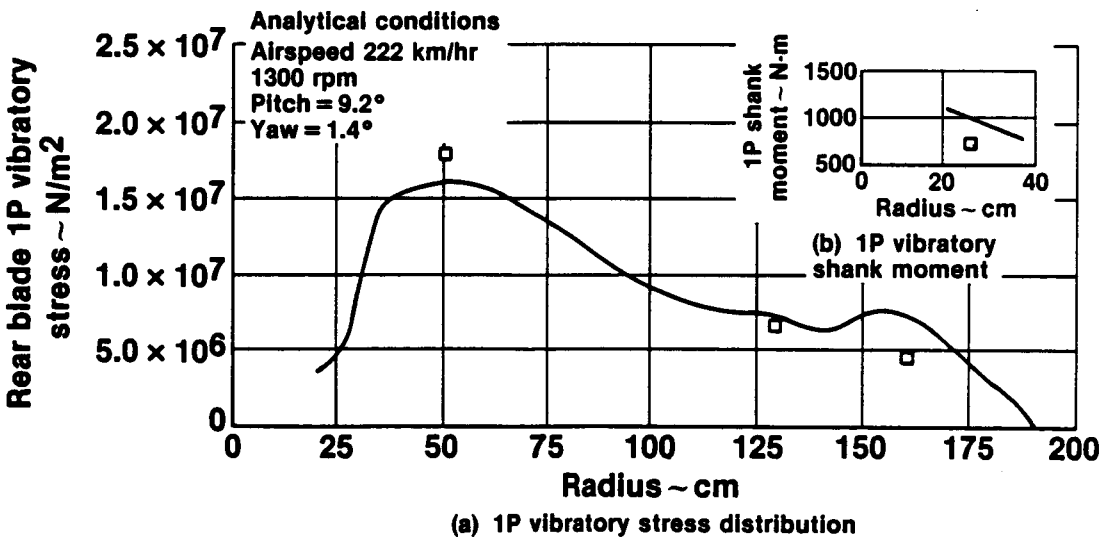


FIGURE 58. COMPARISON OF GANNET REAR BLADE SINGLE ROTATION 1P TEST DATA TO THEORETICAL RESULTS FOR LOW SPEED STABILIZED FLIGHT 222 KM/HR

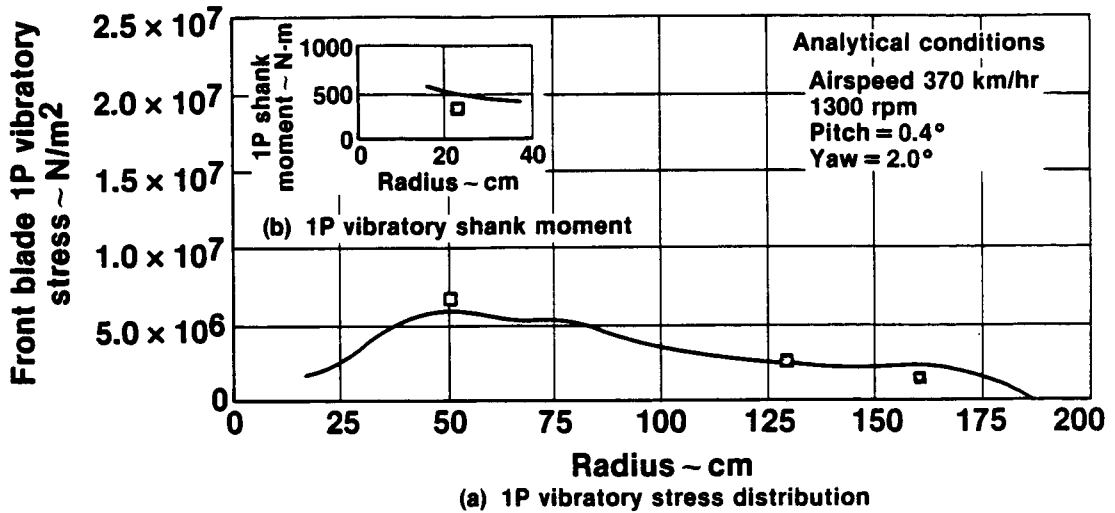


FIGURE 59. COMPARISON OF GANNET FRONT BLADE SINGLE ROTATION 1P TEST DATA TO THEORETICAL RESULTS FOR HIGH SPEED STABILIZED FLIGHT 370 KM/HR

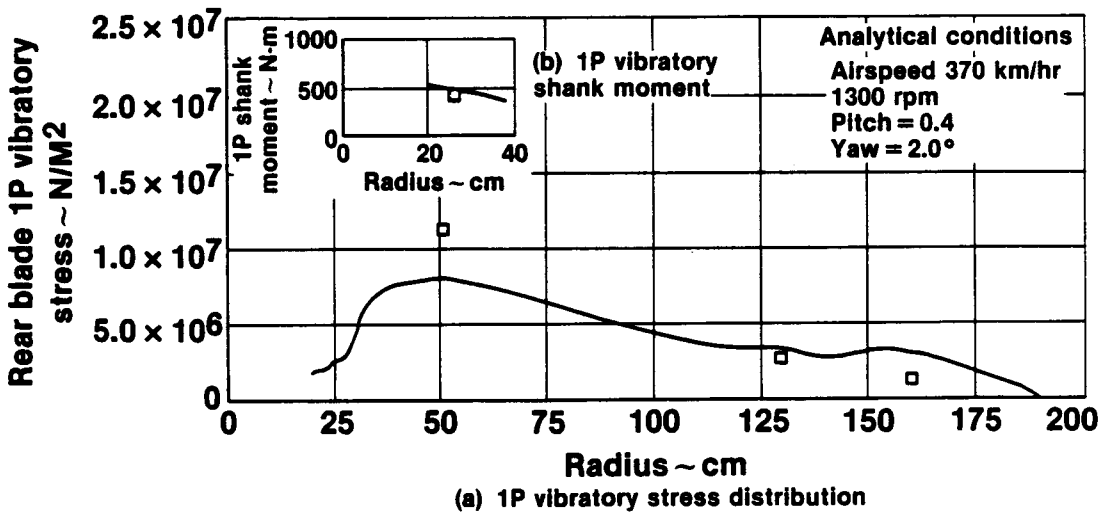
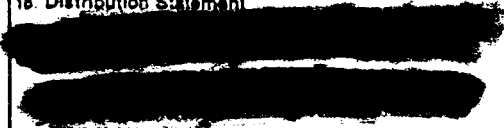


FIGURE 60. COMPARISON OF GANNET REAR BLADE SINGLE ROTATION 1P TEST DATA TO THEORETICAL RESULTS FOR HIGH SPEED STABILIZED FLIGHT 370 KM/HR

1. Report No. CR-174819	2. Government Accession No.	3. Recipient's Catalog No.	
4. Title and Subtitle Effect of Angular Inflow on the Vibratory Response of a Counter-Rotating Propeller		5. Report Date January 15, 1985	
		6. Performing Organization Code	
7. Author(s) J. E. Turnberg P. C. Brown		8. Performing Organization Report No.	
		10. Work Unit No.	
9. Performing Organization Name and Address Hamilton Standard Div., United Technologies Corp. Windsor Locks, CT 06096		11. Contract or Grant No. NAS3-24222	
		13. Type of Report and Period Covered Contractor Report	
12. Sponsoring Agency Name and Address National Aeronautics and Space Administration Lewis Research Center 21000 Brookpark Road Cleveland, OH 44135		14. Sponsoring Agency Code	
		15. Supplementary Notes	
16. Abstract This report presents the results of a propeller vibratory stress survey on the Fairey Gannet aircraft aimed at giving an assessment of the difference in vibratory response between single and counter-rotating propeller operation in angular inflow. The survey showed that counter-rotating operation of the propeller had the effect of increasing the 1P response of the rear propeller by approximately 25 percent over comparable single-rotation operation while counter-rotating operation did not significantly influence the 1P response of the front propeller.			
17. Key Words (Suggested by Author(s)) Blades, Propeller, Counter-Rotation, Vibratory Response		18. Distribution Statement 	
19. Security Classif. (of this report) Unclassified	20. Security Classif. (of this page) Unclassified	21. No. of pages	22. Price*